Correspondence:

D. J. Topping,
dtopping@usgs.gov

Self-Limitation of Sand Storage in a Bedrock-Canyon River Arising From the Interaction of Flow and Grain Size

David J. Topping[1] , **Paul E. Grams[1]** , **Ronald E. Griffiths[1]** , **David J. Dean[1]** , **Scott A. Wright[2]** , **and Joel A. Unema[3]**

[1]Grand Canyon Monitoring and Research Center, Southwest Biological Science Center, U.S. Geological Survey, Flagstaff, AZ, USA, [2]California Water Science Center, U.S. Geological Survey, Sacramento, CA, USA, [3]Arizona Water Science Center, U.S. Geological Survey, Flagstaff, AZ, USA

Abstract Bedrock-canyon rivers tend to be supply limited because they are efficient transporters of sediment and not because the upstream supply of sediment is small. A byproduct of this supply limitation is that the finer alluvium stored in these rivers has shorter residence times and smaller volumes than in alluvial rivers. To improve our understanding of disequilibrium sediment transport and its effect on sand storage in bedrock-canyon rivers, we undertook a 20-year study, synthesized herein, of the Colorado River in Grand Canyon. Despite the large loads for which it was renowned, this river exhibited evidence of natural sand-supply limitation and became the perfect natural laboratory for studying sand transport in a bedrock canyon after upstream dam construction exacerbated this supply limitation. During our study, we made and analyzed an unprecedented ~2.5 million measurements of the suspended and bed sediment. Results indicate that sand storage in this bedrock-canyon river is self-limiting owing to the physical controls of flow and grain size causing negative feedbacks that likely also operate in other bedrock-canyon rivers. Following episodic tributary floods that supply finer sand, sand migrates quickly downstream in the form of a wave in which large systematic changes in bed-sand grain size occur. These grain-size changes cause discharge-independent systematic changes in suspended-sand concentration in excess of a factor of 20. Although the tributary supply of sand increases the amount of sand storage, it also greatly increases the downstream sand transport by causing bed-sand fining, thus limiting the residence time and volume of sand storage.

Plain Language Summary Increases in flow and decreases in sand grain size interact to limit sand storage in bedrock-canyon rivers such as the Colorado River in Grand Canyon. For a given grain size, an increase in flow (i.e., discharge) will cause a large, nonlinear increase in sand transport. Likewise, for a given flow condition, a decrease in grain size (i.e., fining of the bed-sand grain-size distribution) will also cause a large, nonlinear increase in sand transport. In bedrock-canyon rivers where the bed sand is typically coarser than the sand supply, the episodic addition of sand causes temporary fining of the bed sand that produces sand-transport increases that may be as large as those caused by typical flow increases. This grain-size effect causes newly supplied sand to migrate downstream as sand waves, with substantial coupled changes in sand grain size occurring in the bed and in transport. Adding finer sand to a bedrock-canyon river therefore only temporarily increases the sand storage because it also increases the downstream sand transport. Because the downstream transport of sand is increased at higher discharge, increases in flow lead to greater self-limitation of sand storage, and therefore lesser amounts of sand in a bedrock-canyon river like the Colorado River.

1. Introduction

The residence time and storage volume of sand and finer sediment in bedrock-canyon rivers are respectively much shorter and smaller than in alluvial rivers (Bradley & Tucker, 2013; Pizzutto et al., 2017; Skalak & Pizzuto, 2010). These limitations on residence time and storage volume arise because bedrock-canyon rivers are efficient transporters of sediment owing to their extremely nonuniform and highly turbulent flow conditions (Venditti et al., 2014), and because of their restricted accommodation space. Bedrock-canyon rivers therefore tend to be supply limited because they are efficient transporters of sediment (Topping, Rubin, & Vierra, 2000)

despite the fact that some bedrock-canyon rivers transport among the largest sediment loads on Earth (Milliman & Meade, 1983). Understanding the physical interaction of sediment supply and transport that leads to supply limitation is critical for a wide range of theoretical and applied purposes, ranging from studies of landscape evolution to river management. Canyon incision requires at least intermittent exposures of bedrock; thus, it is important to understand the sediment-transport processes that lead to the transient alluvial cover that regulates incision in bedrock-canyon rivers (Sklar & Dietrich, 2001; Whipple et al., 2013, 2000). Moreover, accurate sediment routing through river networks and prediction of drainage-basin evolution requires knowing the physical controls on sediment transport through both supply-limited and transport-limited segments (Howard, 1994). Deposition of finer sediment on gravel substrates may limit riverine biological processes (Cross et al., 2013; Lisle, 1989; Montgomery, 2003; Osmundson et al., 2002), thus also requiring knowledge of the physics that control the transient storage of sand and finer sediment. Finally, it is important to understand the physics that give rise to the natural tendency of bedrock-canyon rivers to be supply limited when managers desire to maximize sand storage in these rivers. This knowledge is especially critical in cases where the natural supply limitation has been exacerbated, e.g., where most of the sand supply has been cutoff by a dam and discharges are relatively high (Schmidt & Wilcock, 2008).

An example of a naturally supply-limited, dam-altered bedrock-canyon river is the Colorado River in Grand Canyon National Park (GCNP; Topping, Rubin, & Vierra, 2000), a UNESCO World Heritage Site. Though occupying a small part of the riverscape, sandbars and other sandy deposits are a characteristic part of the landscape, and are important for habitat, recreation, and archeological-site preservation (East et al., 2016; Schmidt & Grams, 2011; U.S. Department of the Interior, 1995). The construction of Glen Canyon Dam radically changed the flow and sediment conditions of the Colorado River in GCNP. The 1963 closure of this dam cutoff ~95% of the fluvial sand supply at the upstream boundary of GCNP (Topping, Rubin, & Vierra, 2000). Subsequent dam operations largely removed the below-median pre-dam discharges under which sand seasonally accumulated (Topping et al., 2003) and also removed the floods that seasonally scoured this sand from the channel and deposited sandbars (Schmidt, 1990). Public recognition that dam operations were causing net erosion of sandbars in the early 1970s (Dolan et al., 1974) led to intensive study beginning in the 1980s (Carothers & Brown, 1991), and culminated in the passage of the Grand Canyon Protection Act (1992). This law directed that Glen Canyon Dam be managed to "protect, mitigate adverse impacts to, and improve the values" for which GCNP was established. River managers thereupon tasked scientists with developing dam reoperation plans to retain sufficient sand in the Colorado River in GCNP to sustainably rebuild sandbars (U.S. Department of the Interior, 1995, 2016a). Though some earlier studies reached a different conclusion (e.g., Laursen et al., 1976), the presumption by the mid-1990s was that tributary-supplied sand accumulated on the riverbed over multiyear timescales downstream from Glen Canyon Dam and could be used to rebuild sandbars during episodic dam-released controlled floods (U.S. Department of the Interior, 1995, 1996). Research following the first controlled flood in 1996 (Webb et al., 1999), however, showed that the river was instead sand-supply-limited and that long-term sand accumulation was unlikely owing to large changes in sand transport associated with changes in grain size (Rubin et al., 2002; Topping, Rubin, Nelson et al., 2000; Topping, Rubin, & Vierra, 2000).

Therefore, the U.S. Geological Survey (USGS) began a program of intensive suspended-sediment measurements in 1998 to better understand the disequilibrium sediment transport that dominates in the Colorado River, and that is likely a defining characteristic of bedrock-canyon rivers. This work led to the design of controlled floods to follow and utilize new tributary sand inputs (Grams et al., 2015; Rubin et al., 2002; Wright & Kennedy, 2011; Wright et al., 2008) and also led to modified nonflood dam operations (U.S. Department of the Interior, 2016a, 2016b). To date, our USGS program has made over 2.5 million suspended-sediment measurements (~1.7 million that include sand grain size) and ~1,600 bed-sediment measurements. This paper both synthesizes earlier learning and presents new results from this 20-year ongoing research effort.

1.1. Study Area

Our study was conducted in the Colorado River and its tributaries between Glen Canyon Dam and Lake Mead from 1996 through 2017 (Figure 1). For sand-budgeting purposes, we divide the Colorado River into five major segments: Upper Marble Canyon (UMC), Lower Marble Canyon (LMC), Eastern Grand Canyon (EGC),
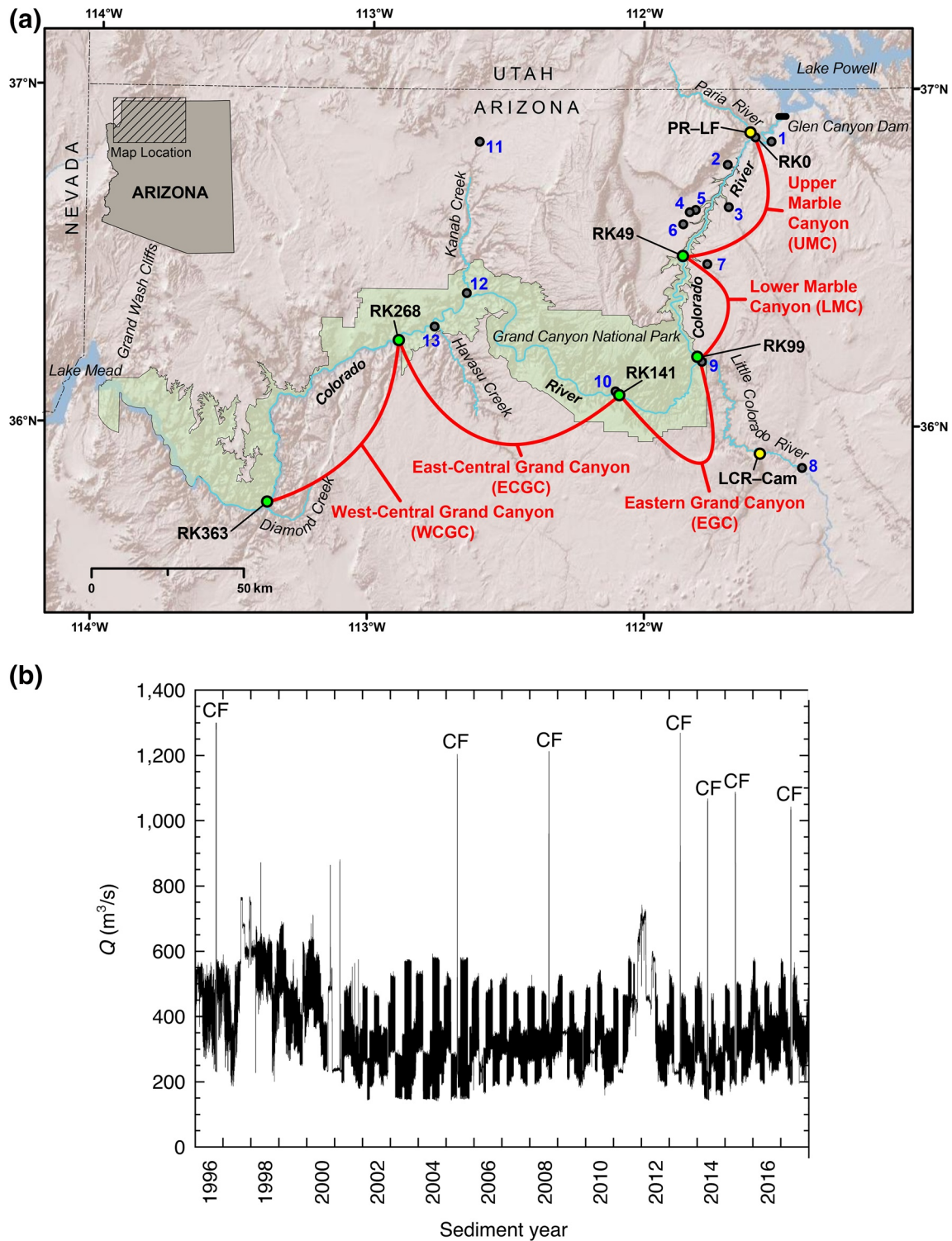
Figure 1. Study area map showing the gaging stations where continuous suspended-sediment measurements (green circles) and event-based sampling (yellow circles) were used to calculate 15-min loads for sand budgeting in the bracketed segments (depicted in red). Lower Glen Canyon extends from Glen Canyon Dam to the Paria River; Marble Canyon extends from the Paria River to the Little Colorado River (LCR); Grand Canyon extends from the LCR to the Grand Wash Cliffs. "PR–LF" indicates the Paria River at Lees Ferry gaging station; "LCR–Cam" indicates the LCR near Cameron gaging station. Blue numbers indicate the other stations used in our study, abbreviated as: (1) Water Holes Canyon, (2) Badger Creek, (3) Tanner Wash, (4) House Rock Wash, (5) House Rock Wash in Rider Canyon, (6) North Canyon, (7) Shinumo Wash, (8) LCR at Cameron, (9) LCR–mouth, (10) Bright Angel Creek, (11) Kanab Creek–Fredonia, (12) Kanab Creek–mouth, and (13) Havasu Creek. (b) Instantaneous discharge (Q) at the RK0 station during the period of our study; CF indicates controlled flood.

East-Central Grand Canyon (ECGC), and West-Central Grand Canyon (WCGC). We refer to ~1-km-long river sections as a "reach," and longer sections as a "segment." Longitudinal distances along the Colorado River are measured downstream from the RK0 station; RK is short for "river kilometer." The five segments are bracketed by USGS gaging stations abbreviated herein as the RK0, RK49, RK99, RK141, RK268, and RK363 stations. Official USGS and abbreviated names of all gaging stations are listed in Text S1. We use the July 1 through June 30 "sediment year" of Topping, Rubin, and Vierra (2000), defined such that each year begins with the season of maximum tributary sediment supply (July 1 of preceding calendar year) and ends with the natural season of maximum sediment export, that is, the pre-dam snowmelt flood (June 30 of current calendar year).

Most of the Colorado River in our study area is a gravel-bedded pool-drop river, and this morphology controls the loci of sand storage. Boulder-dominated debris fans at tributary mouths constrict the river and form rapids (Dolan et al., 1978; Howard & Dolan, 1984). Lower-gradient pools form upstream from these rapids, and lateral-recirculation eddies form in the downstream flow expansion. Sand is stored in both of these environments and in channel-margin bank deposits (Rubin et al., 1990; Schmidt, 1990; Schmidt & Graf, 1990; Schmidt & Rubin, 1995; Schmidt et al., 1999). Depending on pool geometry, sand may completely cover the bed or occur in relatively small, thin patches on a gravel-bedrock substrate (Grams et al., 2013). The greatest sand thicknesses generally occur in sandbars in the eddies downstream from the rapids (Barnhardt et al., 2001; Hazel et al., 2006; Platt, 2018; Rubin et al., 1994). Although the sand grain size generally fines from lower elevations on the channel bed to higher elevations in the eddies and on the banks (Hazel et al., 2006; Rubin et al., 2020), individual sand deposits tend to be inversely graded. In higher-elevation deposits, this inverse grading occurs both within the sand-size sediment and also in the silt and clay, arising from the progressive depletion of the upstream sediment supply during pre-dam snowmelt floods and during dam-released controlled floods (Draut & Rubin, 2013; Rubin et al., 1998; Topping, Rubin, & Vierra, 2000; Topping, Rubin, Nelson et al., 2000; Topping et al., 2005, 2006). Inverse grading of channel-bed sand (armoring) is likely present during periods of combined high mainstem discharge and tributary quiescence, when progressive depletion of the upstream sand supply leads to bed-sand winnowing (Rubin et al., 1998; Topping, Rubin, Nelson et al., 2000; Topping, Rubin, & Vierra, 2000; Topping et al., 2005; Topping et al., 2010, 1999). Despite the tributaries supplying a large amount of silt and clay, the silt and clay content in the bed is generally negligible except in eddies (Hazel et al., 2006). Although the silt and clay content in the channel bed does increase following tributary floods (Figure 14 in Topping, Rubin, Nelson et al., 2000), large increases in silt and clay are restricted to eddies, where we have observed silt and clay to comprise as much as ~17% of the bed following large tributary floods.

1.2. Colorado River Sand-Transport Synthesis

Sand transport in rivers is controlled by the interaction of the upstream sand supply with the flow and the sand locally available on the bed, bars, and banks. Water discharge (Q), influences the cross-section-integrated sand flux (Q_{SAND}) through a river cross section on a spatially, reach-averaged basis primarily through the boundary shear stress (τ_b), and secondarily through the flow velocity, depth, and width (Grams et al., 2013). In this usage, "cross-section-integrated flux" refers to the surface integral of the local flux over each point in the river cross section. The upstream sand supply influences Q_{SAND} primarily through the bed-sand grain-size distribution, and secondarily through the areal fraction of the bed covered by sand (i.e., bed-sand area), and scour-and-fill driven variation in τ_b (Rubin et al., 2020), as elaborated upon below. Under equilibrium sand transport, the bed-sand grain-size distribution remains constant because the upstream supply and downstream export of each sand size class are in balance across all Q. Under this condition, negligible variation exists when the velocity-weighted suspended-sand concentration (C_{SAND}) is plotted as a function of Q; an increase in Q causes an increase in τ_b that, in turn, causes an increase in both C_{SAND} and the suspended-sand median grain size (D_S), with the highest values of C_{SAND} associated with the largest values of D_S. This scenario is commonly called the "transport-limited" case in the literature (Dietrich et al., 2003; Howard, 1994), a scenario we refer to as "flow-regulated" (following Rubin & Topping, 2001). Conversely, under disequilibrium sand transport, the upstream supply and downstream export of each sand size class are not in balance across all Q. Under this supply-limited condition, changes in the upstream sand supply cause changes in the bed-sand grain-size-distribution that may completely offset the influence of Q on C_{SAND}. In a completely supply-limited case, the highest values of C_{SAND} are associated with the

smallest values of D_S and not the largest values of Q, a scenario we refer to as "grain-size-regulated" (following Rubin & Topping, 2001).

Tributary floods have a much larger effect on the upstream sediment supply than they do on Q in the Colorado River. Most tributary floods are of short duration (Dean & Topping, 2019; Griffiths & Topping, 2017; Melis et al., 1996; Topping, 1997) and supply relatively small amounts of water compared to the Q released from Glen Canyon Dam (Rubin et al., 2020). Consequently, dam operations largely determine Colorado River Q throughout our study area. The suspended-sediment concentrations during these tributary floods, however, are among the highest measured in the world (Beverage & Culbertson, 1964; Dean & Topping, 2019; Griffiths & Topping, 2017; Topping, 1997) and the tributary sand tends to be much finer than the antecedent bed sand in the Colorado River (Topping, Rubin, Nelson et al., 2000).

The sediment supplied during a tributary flood is transported downstream in the Colorado River as an elongating sediment wave with components in transport and on the bed (Topping, Rubin, Nelson et al., 2000). Owing to the lower Rouse numbers of the finer sediment size classes, progressively more of these size classes are in transport and not temporarily stored in the bed (after Rouse, 1937; McLean, 1992) during downstream wave migration. The sediment waves consequently undergo segregation by grain size. Because the silt-and-clay-sized sediment are transported as washload (Einstein et al., 1940; Woo et al., 1986) and have only minimal representation in the bed, they form a silt-and-clay wave that is almost entirely in transport. The sand-size sediment forms a lagging sand wave with progressively greater representation in the bed of the coarser size classes, as governed by physical suspension processes (McLean, 1992) and the lower flux boundary condition for suspended sediment (Parker, 1978). Our observations in the late 1990s suggested that the sand waves further split into two "packets" as they travel downstream, with packet A leading packet B (Text S2). Packet A migrated quickly downstream with celerity slightly slower than the velocity of the water (Topping, Rubin, Nelson et al., 2000). As it migrated downstream, packet A left behind a longitudinally discontinuous very fine secondary mode in the bed sand that decayed in amplitude in the downstream direction (Figure 14 in Topping, Rubin, Nelson et al., 2000). Packet B presented as a unimodal sand bed that blanketed the antecedent coarser sand and gravel bed. Packet B fined in the upstream direction from the front ($D_{50} = 0.44$ mm) to the peak ($D_{50} = 0.11$ mm), and then coarsened in the upstream direction from the peak to the tail ($D_{50} = 0.30$ mm). The median grain size of the bed sand at the peak of packet B (0.11 mm) was slightly coarser than the secondary mode (0.096 mm) that comprised the bed component of packet A (Figure 14 in Topping, Rubin, Nelson et al., 2000).

Sand-wave migration is associated with coupled changes in C_{SAND} and the suspended- and bed-sand grain-size distributions, and also inferred changes in reach-averaged bed-sand area and τ_b as the channel fills and scours. As required by the flux lower boundary condition of Parker (1978), the tributary introduction of a large amount of finer suspended sand causes an overloaded disequilibrium sand-transport condition in the Colorado River, that is, a condition where the suspended-sand concentration and grain-size distribution are respectively higher and finer than that in equilibrium with the antecedent bed-sand grain-size distribution. This overloaded condition causes a net flux of sand from suspension to the bed, causing the bed sand to fine (Topping et al., 2007). The subsequent decrease in upstream sand supply as tributary flooding ceases gives rise to the opposite, underloaded condition. A net flux of sand from the bed to suspension then occurs, leading to a coarsening of the bed-sand grain-size distribution by winnowing the finest size classes from the bed (Rubin et al., 1998). Within sand waves, the bed-sand grain-size distribution thus fines in the upstream direction in the leading edge (from the front of a wave to the peak), and the bed-sand grain-size distribution coarsens in the upstream direction in the trailing edge (from the peak to the tail).

Bed-sand grain size exerts a strong nonlinear control on C_{SAND} (Rubin & Topping, 2001, 2008; Topping, Rubin, Nelson et al., 2000; Topping et al., 2007), whereas bed-sand area exerts a weaker quasi-linear control on C_{SAND} (Grams & Wilcock, 2007, 2014; Topping et al., 2007). Consequently, changes in bed-sand grain size are the dominant bed signature of the changes in upstream sand supply associated with sand-wave migration (Topping et al., 2018). Changes in bed-sand area associated with sand-wave migration are likely to be relatively small, except in the reach downstream from the sand-wave-generating tributary, where transient orders-of-magnitude changes in bed-sand area have been observed (Topping, Rubin, Nelson et al., 2000). Repeat maps of the Colorado River show that there is less than a factor of ~2 variation in bed-sand area during periods of tributary quiescence, and that sand patches tend to be topographically "locked" under similar flow conditions (Grams

et al., 2019, 2013). This behavior arises because sand patches are largely determined by local convergence (i.e., a spatial decrease) in τ_b caused by the interaction of the flow with the bed topography (Topping, Rubin, Nelson et al., 2000). Because the loci of convergence in τ_b may change as a function of Q, sand patches may, however, be located on different parts of the bed under different flow conditions. Large increases in Q tend to redistribute sand from deep pools to larger areas of the bed (Topping, Rubin, Nelson et al., 2000), but sand slowly recollects in the pools after Q decreases. Consequently, sand patches have been observed on different parts of the gravel-bedrock substrate at different Q, with large increases in Q causing up to a factor of ~3 increase in bed-sand area (Anima et al., 1998; Schmidt et al., 2007). Thus, sand-wave migration likely causes much less than a factor of 10 change in sand-patch area except in the reaches proximal to flooding tributaries, where gravel beds can be temporarily converted to sand beds (Topping, Rubin, Nelson et al., 2000). Owing to the quasi-linear control of bed-sand area on C_{SAND}, changes in sand-patch area associated with sand-wave migration are therefore inferred to be associated with less than an order-of-magnitude change in C_{SAND} (Topping et al., 2007). In contrast, half-order-of-magnitude changes in bed-sand median grain size (D_B) cause several orders of magnitude change in C_{SAND} (Topping et al., 2007; Topping, Rubin, Nelson et al., 2000). Changes in bed-sand grain size can thus completely offset the sometimes-opposing control of bed-sand area on C_{SAND} (Topping et al., 2007); accordingly, changes in bed-sand area are neglected in our analyses.

Q-independent changes in reach-averaged τ_b caused by fill and scour during sand-wave migration are also less important than the control of bed-sand grain size on C_{SAND}, and for the purposes of our analyses are also neglected. The location of a sand patch on the bed is determined by convergence in τ_b, and a patch will aggrade and enlarge in the presence of an increased upstream sand supply during sand-wave migration until the convergence disappears and that part of the bed ceases to be a depositional environment (Topping, Rubin, Nelson et al., 2000). Large increases in sand-patch thickness will therefore cause an increase in the spatially averaged τ_b over a patch, thus leading to an increase in the reach-averaged τ_b. Bed-sand area is generally 10%–70% over the reach scale (Anima et al., 1998; Grams et al., 2019, 2013; Schmidt et al., 2007; Topping et al., 2007) and substantial changes in sand-patch thickness are localized. For example, between 2009 and 2012, 70% of the total change in sand volume in a 50-km river segment occurred over only 12% of the length of this segment (Grams et al., 2019). The changes in the spatially averaged τ_b over patches caused by fill and scour during sand-wave migration are thus likely to be <<100% in reaches distal to tributaries. These local changes will therefore cause a change in reach-averaged τ_b of <50% (Topping et al., 2010). Because the shear velocity $u_* = \sqrt{\tau_b / \rho}$ (where ρ is water density), this maximum likely change in τ_b corresponds to only a factor of ~1.2 change in u_*, the maximum variation in reach-averaged u_* confirmed by measurements (Text S3). This level of variation in reach-averaged u_* causes only a factor of ~2 change in C_{SAND}, much less than the factor of >20 change in C_{SAND} caused by changes in bed-sand grain size (after Rubin & Topping, 2001; Topping et al., 2007; Text S4).

2. Field Methods

We measured suspended sediment in the Colorado River using a combination of the following five methods: Equal-Discharge-Increment (EDI), Equal-Width-Increment (EWI), Velocity-weighted-average Point-sample Array (VPA; Edwards & Glysson, 1999), calibrated-pump (Topping et al., 2010), and acoustical (Topping & Wright, 2016; Text S4). Before 2002, measurements were made episodically using depth- and point-integrating suspended-sediment samplers deployed in the EDI, EWI, or VPA methods. Beginning in 2002, measurements were made at 15-min intervals at four stations using single-frequency acoustic-Doppler profilers (ADPs) augmented by pump samples calibrated using EDI/EWI measurements. One additional station and ADPs at additional frequencies were added over time such that, by 2008, acoustical methods using two or three frequencies were used to measure the velocity-weighted suspended-silt-and-clay concentration ($C_{SILT-CLAY}$), C_{SAND}, and D_S at 15-min intervals in the river cross sections at five stations (Griffiths et al., 2012). Acoustical measurements were calibrated and subsequently verified using EDI/EWI measurements and EDI/EWI-calibrated-pump measurements (Topping & Wright, 2016). Bed-sediment measurements were generally made on the same days as the EDI/EWI measurements and typically consisted of three to five samples collected across the cross-section. No bed-sediment measurements were made at the largely gravel-bedded RK0 station. Laboratory methods for processing samples are described by Topping et al. (2010).

To better constrain the sediment supply to the Colorado River, we made extensive suspended-sediment measurements in the tributaries (Figure 1). Event-based sampling using EWI, EDI, single-vertical, and calibrated-pump measurements was conducted in the Paria River at the PR–LF station and Little Colorado River (LCR) at the LCR–Cam station. Beginning in 2000, this effort included new gaging stations and automatic samplers in a subset of the formerly ungaged lesser tributaries (Griffiths & Topping, 2017; Griffiths et al., 2014). This effort was expanded again to include Bright Angel Creek in 2005, and Kanab and Havasu creeks in 2010. Owing to the remoteness of all tributaries except the Paria River and LCR, suspended-sediment measurements in these other tributaries were mostly made by calibrated automatic samplers. All data collected for this study, with user-interactive plots and sediment budgets, are available at: https://www.gcmrc.gov/discharge_qw_sediment/ (Sibley et al., 2015).

All of the suspended-sediment measurements have known field and laboratory errors (Topping et al., 2010, 2011). Errors in calibrated-pump suspended-sand measurements are larger than those in EDI/EWI measurements, and depend on intake-tube length, pumped sample volume, C_{SAND}, and grain size (Topping et al., 2010). Relative error in individual acoustical measurements of C_{SAND} decreases with increasing C_{SAND}, whereas relative error in individual acoustical measurements of D_S is constant (Topping & Wright, 2016; Topping et al., 2016).

3. Analytical Methods

3.1. Instantaneous Cross-Section-Integrated Sand Fluxes and Cumulative Sand Loads

Q_{SAND} is the sum of the cross-section-integrated suspended- and bedload-sand fluxes. The local suspended-sand flux at each point in a cross section is the product of the local flow velocity and suspended-sand concentration. Because the cross-section-integrated suspended-sand flux is the surface integral of the local suspended-sand flux over each point in the cross section, it is equivalent to the product of the velocity-weighted suspended-sand concentration in the river cross section (i.e., C_{SAND}) and Q, that is, the standard method (Guy, 1970) we used to calculate the cross-section-integrated suspended-sand flux at each 15-min interval. The cross-section-integrated bedload-sand flux in the Colorado River was estimated as 5% of the cross-section-integrated suspended-sand flux on the basis of dune-migration measurements at the RK99 and RK141 (Rubin et al., 2001) and RK363 stations (Ashley et al., 2020). The shifting-rating-curve method (Topping et al., 2018, 2010) was used in conjunction with suspended-sediment measurements and Q to calculate Q_{SAND} in the Paria River and LCR, and in Kanab and Havasu creeks: linearly shifting the relation between Q and C_{SAND} over time so that the rating-curve predictions of C_{SAND} equaled the measured C_{SAND} at the time of each suspended-sediment measurement. Although the cross-section-integrated bedload-sand flux was found to be negligible in the Paria River and LCR (owing to low Rouse numbers), model estimations of bedload sand transport were included in the calculations of Q_{SAND} in these two rivers (after Topping, 1997). Bedload sand transport was neglected in all other tributaries on the basis of this result. For the post-2002 period of 15-min Q_{SAND} at the five Colorado River stations, the post-1997 period of 15-min Q_{SAND} in the Paria River and LCR, and the post-2010 period in Kanab and Havasu creeks, sand loads were calculated by integrating these data over time (after Porterfield, 1972). This method was also used at the RK0 station, where C_{SAND} was typically measured only during controlled floods. Methods used for Q_{SAND} and sand loads in the gaged subset of lesser tributaries are described in Griffiths and Topping (2017), and for all lesser tributaries in Text S5. Cross-section-integrated silt-and-clay fluxes and loads were calculated using the same methods as for sand. Annual sand and silt-and-clay loads at all stations are provided in Text S6.

Uncertainties in sand loads were estimated on the basis of the maximum likely magnitudes of small persistent biases in the measurements of C_{SAND} (e.g., Sabol & Topping, 2013; Topping et al., 2010) and Q (e.g., Kiang et al., 2016; Sauer & Meyer, 1992). Thus, 5% uncertainties were assigned to Colorado River loads calculated from the 15-min suspended-sand data. Owing to the larger possible persistent biases in the Q records and from use of the shifting-rating curve method, 10% uncertainties were assigned to loads in the Paria River and in the LCR (at LCR–Cam), and 20% uncertainties were assigned to loads calculated using the shifting-rating curve method on the sparser suspended-sand data in Kanab Creek, Havasu Creek, and elsewhere in the LCR. 50% uncertainties were assigned to lesser-tributary loads.

3.2. Discharge Versus Sand-Supply Control of Sand Transport

We evaluated the relative importance of Q versus the upstream sand supply in controlling sand transport in the Colorado River using α, a nondimensional index derived from suspended-sediment theory by Rubin and Topping (2001). Bed-sand grain size was used as a proxy for the upstream sand supply, as justified in Section 1.2.

$$\alpha = \left(\frac{K}{J+1}\right)\left(\frac{\log_{10} \Delta D_{\mathrm{B}}}{\log_{10} \Delta u_*}\right) = \left(\frac{K}{J+1}\right)\frac{-L\left(\dfrac{\log_{10} \Delta C_{\mathrm{SAND}}}{\log_{10} \Delta D_{\mathrm{S}}}\right) + J}{M\left(\dfrac{\log_{10} \Delta C_{\mathrm{SAND}}}{\log_{10} \Delta D_{\mathrm{S}}}\right) - K} \tag{1}$$

is a quantitative measure of the relative importance of u_* versus D_{B} in regulating sand transport. The values of J, K, L, and M in Equation 1 are derived from theory (Rubin & Topping, 2001) and vary as a function of the bed-sand sorting and whether dunes are present. The bed sand of the Colorado River in our study area is generally well-sorted, with a mean geometric standard deviation (GSD) of 0.53ϕ (Text S7). Dunes are not always present on the bed owing to changing sand-patch thickness and flow conditions. Thus, the mean values derived by Rubin and Topping (2001) for well-sorted bed sand (GSD = 0.55ϕ) among cases with and without dunes, $J = 4.3$, $K = -2.8$, $L = 0.18$, and $M = 0.85$, are used in Equation 1. Δ in Equation 1 signifies the ratio of either C_{SAND} or D_{S} at two different times. To apply Equation 1 to our large datasets, with many hundreds of thousands of measurements, we use the approximation of Rubin and Topping (2001):

$$\left|\frac{\log_{10} \Delta C_{\mathrm{SAND}}}{\log_{10} \Delta D_{\mathrm{S}}}\right| \approx \frac{\sigma\left(\log_{10} C_{\mathrm{SAND}}\right)}{\sigma\left(\log_{10} D_{\mathrm{S}}\right)} \tag{2}$$

where σ indicates the standard deviation. We then use the method of Topping et al. (2018) to evaluate the sign of $\log_{10} \Delta C_{\mathrm{SAND}} / \log_{10} \Delta D_{\mathrm{S}}$ and calculate $|\alpha|$. We calculated $|\alpha|$ separately for the EDI/EWI/VPA, calibrated-pump, and acoustical suspended-sand measurements owing to the different error magnitudes between these three measurement types.

α is defined such that u_* is more important than D_{B} in regulating sand transport when $|\alpha| < 1$ and D_{B} is more important than u_* in regulating sand transport when $|\alpha| > 1$. Steady, uniform-flow estimation of u_* from Q measurements (Text S3) indicates that the positive correlation between cross-section average u_* and Q is nearly perfect in the Colorado River (with correlation coefficient $r \geq 0.97$). Thus, $|\alpha|$ is also a quantitative measure of the importance of changes in Q versus changes in D_{B} in regulating C_{SAND}. This result indicates that when $|\alpha|$ approaches zero, C_{SAND} is insensitive to changes in the upstream sand supply and is controlled only by changes in Q (i.e., the flow-regulated case), whereas C_{SAND} is completely controlled by changes in the upstream sand supply when $|\alpha|$ approaches infinity (i.e., the grain-size regulated case).

3.3. Bed-Sand Grain Size

To take advantage of our 1.7 million measurements of suspended-sand concentration and grain size, and not be analytically limited by relatively sparse bed-sediment measurements (typically between only 4 and 10 per year at each station), we back-calculated the reach-averaged bed-sand grain size in the Colorado River from the suspended-sand data using the nondimensional β derived from theory by Rubin and Topping (2001, 2008). This approach allowed us to develop time series of reach-averaged bed-sand grain size with high temporal resolution that were then analyzed to determine the effects of Q and the tributary resupply of sand on the Colorado River bed sand over timescales of 15 min to decades.

$$\beta = \left(\frac{C_{\mathrm{SAND}}}{C_{\mathrm{SAND-REF}}}\right)^{-0.1}\left(\frac{D_{\mathrm{S}}}{D_{\mathrm{S-REF}}}\right) \tag{3}$$

is a measure of the relative coarseness of the bed sand, where C_{SAND} is from a single measurement, $C_{\mathrm{SAND-REF}}$ is the reference C_{SAND}, D_{S} is from a single measurement, and $D_{\mathrm{S-REF}}$ is the reference D_{S}. Reference values

are mean values over an entire dataset (Text S7), such that the bed sand is finer than the mean condition when $\beta < 1$. We calculated β for the three suspended-sand measurement types (i.e., EDI/EWI/VPA, calibrated-pump, and acoustical) using values of $C_{\text{SAND-REF}}$ and $D_{\text{S-REF}}$ at each station from only the EDI/EWI/VPA measurements. We used this approach because the EDI/EWI/VPA measurements (made with isokinetic depth- and point-integrating suspended-sediment samplers) provided the most accurate measurements of C_{SAND} and D_{S}. In addition, this approach allowed the β values at each station to be consistent between the three measurement types. C_{SAND} commonly varies by ~1.5 orders of magnitude and D_{S} commonly varies by a factor of ~1.5 in the Colorado River. Therefore, even though D_{S} is raised to a power 10 times larger than C_{SAND} in Equation 3, changes in C_{SAND} and D_{S} tend to equally influence β in the Colorado River in our study area.

The bed-sand grain-size metric tracked by β depends on the transport mode for the majority of the bed sand. When most of the bed-sand grain-size distribution is transported in suspension (i.e., the Rouse number for $D_{\text{B}} < 1$), $\beta = D_{\text{B}}/D_{\text{B-REF}}$ by definition, where $D_{\text{B-REF}}$ is the mean D_{B} over the entire dataset (Rubin & Topping, 2001, 2008; Topping et al., 2010; Text S7). However, when a large part of the bed-sand grain-size distribution is transported as bedload, β can be uncorrelated with D_{B} and only relate to the amount of finer sand on the bed (Topping et al., 2018). By the physics that govern suspended sediment, the fractional amount (*f*) of a sand size class on the bed surface required to support a given amount of sand in suspension increases nonlinearly with grain size (after McLean, 1992). Consequently, relations between β and *f* in the fine tail of the bed-sand grain size distribution are semi-logarithmic such that $\beta \propto -\log(f)$; these relations have negative slopes and correlations that decrease as grain size increases (Text S2). Thus, β is most sensitive to changes in the fractional amount of the finest sand on the bed.

β should be more representative of the reach-averaged bed-sand grain-size distribution in a river than are direct bed-sediment measurements made at only one cross-section. Because suspended sand equilibrates with the bed over the 100s-of-m to 1-km reach scale in the Colorado River (Topping et al., 2007), the β-calculated bed-sand grain size is that which is "sampled" by the physical processes governing suspended sand over these larger spatial scales. The bed-sand grain-size distribution in the main channel at one cross-section does not necessarily correlate well with the reach-averaged bed-sand grain-size distribution in equilibrium with the suspended sand. Over decade-plus timescales, the suspended sand in the Colorado River has been regulated more strongly by changes in the grain-size distribution on the eddy-sandbar surfaces than by changes in the grain-size distribution of the sand on the channel bed, despite eddies comprising only ~20% of the inundated area of the Colorado River (Topping et al., 2005, 2008).

Support for β as an accurate measure of the reach-averaged bed-sand grain size is provided by the C-run flume experiments of Einstein and Chien (1953b). In these experiments, where the D_{B} Rouse number ranged from ~0.4 to 0.6, the upstream sediment supply was systematically varied to utilize the physical suspension processes to form a bed surface in equilibrium with the suspended sediment. Einstein and Chien measured the equilibrium bed surface at two sections in the flume; hence their bed-surface grain-size distributions are spatial averages. For these experiments, the $D_{\text{B-REF}}$ back-calculated using regression from $\beta = D_{\text{B}}/D_{\text{B-REF}}$ differs from the true $D_{\text{B-REF}}$ among the measured D_{B} values by only 4%. Moreover, the correlations between β and D_{B} for sand-size sediment and between β and the log-transformed fractional amount of very fine (0.0625–0.125 mm) bed sand (f_{VF}) are nearly perfect, with *r* values of 0.98 and −0.99, respectively. Because these values correspond to respective R^2 values of 0.96 and 0.98, β thus explains most of the variance in bed-sand grain size in this well-constrained dataset. Therefore, weaker correlations between β and bed-sand grain size in rivers likely arise, not from physical simplifications in the derivation of β, but rather from sparser bed-sediment measurements in rivers being less representative than β of the reach-averaged bed sand "sampled" by the suspended sand. In addition, although β was derived for sand-covered beds, it provides a reasonably accurate measure of the bed-sand grain size under conditions where sand covers a smaller part of the bed and/or the bed-sand area changes over time. Because bed-sand grain size exerts a much stronger control on C_{SAND} than does bed-sand area, a factor of two change in bed-sand area biases β by only ~7% (Topping et al., 2010).

However, the accuracy of β is limited by the accuracy of the suspended-sand measurements used to calculate β. Though all of the suspended-sediment measurement types used in our study are unbiased (Topping et al., 2010, 2011; Topping & Wright, 2016), only the episodic EDI/EWI/VPA measurements have relatively

small random error (Topping et al., 2011). Although the continuous 15-min acoustical suspended-sand measurements are the only measurements that capture the full range of C_{SAND} and D_{S}, these measurements have the largest random error (Topping & Wright, 2016). The random errors in the EDI/EWI/VPA and acoustical measurements of C_{SAND} decrease substantially as C_{SAND} increases (Topping & Wright, 2016). Thus, the C_{SAND}-weighted mean error in C_{SAND} was chosen to represent the central tendency of the error distribution in C_{SAND} at each station. For individual EDI/EWI/VPA measurements, the mean 95%-confidence-level relative errors averaged among the Colorado River stations are ±12% for C_{SAND} and ±10% for D_{S}. For individual acoustical measurements, the mean 95%-confidence-level relative error averaged among the Colorado River stations are ±69% for C_{SAND} and ±34% for D_{S}. Propagation of these errors through Equation 3 using the methods on pages 61 and 66 in Taylor (1997) indicates that the 95%-confidence-level relative errors in individual values of β are typically ±10% for EDI/EWI/VPA measurements and ±35% for acoustical measurements. Moreover, because the relative error in measured C_{SAND} decreases with increasing C_{SAND}, the relative error in β is lower than these values under the conditions of higher sand transport that exert greater influence in the lagged-covariance and sand-budgeting analyses herein.

3.4. Lagged-Covariance Analyses

We detected the downstream migration of tributary-generated sand waves in the Colorado River over 15-min to annual timescales through analyses of the lagged covariance, that is, cross-covariance (Emery & Thomson, 2001), of tributary Q_{SAND} and Colorado River bed-sand grain size. These analyses utilized the 15-min Q_{SAND} values in the Paria River and LCR, and the 15-min multifrequency acoustical measurements of C_{SAND} and D_{S} in the Colorado River made during sediment years 2008–2017. In these analyses, Δt is equal to 15 min and the cross covariance of A and B at each lag $j\Delta t$ is:

$$\widehat{\mathrm{cov}}_{\mathrm{AB}}\left(j\Delta t\right) = \frac{1}{N-j}\sum_{i=1}^{N-j}\left(A_{\mathrm{i}} - \bar{A}\right)\left(B_{\mathrm{i+j}} - \bar{B}\right) \tag{4}$$

where A_{i} is Q_{SAND} in either the Paria River (at the PR–LF station) or LCR (at the LCR–Cam station) and B_{i} is the value of $1/\beta_{\mathrm{Q}}$ at a station on the Colorado River at a given 15-min interval i. $\bar{A}$ and $\bar{B}$ are the means of A_{i} and B_{i}, respectively, over all N 15-min intervals in the 10 years of data; $j = 0$ through 35,039 because there are 35,040 15-min intervals in a common year. The inverse of Q-detrended β, that is, $1/\beta_{\mathrm{Q}}$, is used so that increasing $\widehat{\mathrm{cov}}_{\mathrm{AB}}\left(j\Delta t\right)$ is associated with bed-sand fining; the reasoning behind using Q-detrended β is explained in Section 4.3. Changes in the bed-sand grain-size distribution require either erosion or deposition of sand. Therefore, the location of a minimum in bed-sand grain size indicates the location of a maximum in sand-wave thickness, that is, the peak of a sand wave or sand-wave packet. Because peaks in $\widehat{\mathrm{cov}}_{\mathrm{AB}}\left(j\Delta t\right)$ indicate a minimum in bed-sand grain size, the time of maximum $\widehat{\mathrm{cov}}_{\mathrm{AB}}\left(j\Delta t\right)$ indicates the time of the peak of a sand-wave packet. Maximum $\widehat{\mathrm{cov}}_{\mathrm{AB}}\left(j\Delta t\right)$ likely reflects maximum f_{VF} and not minimum D_{B} because β is most sensitive to changes in the fractional amount of the finest sand on the bed. To test the utility of this method for detecting sand-wave migration and to evaluate whether large tributary floods occurring in different seasons within the same year would complicate the results, we conducted similar lagged-covariance analyses for silt and clay and additional analyses for sand (Text S8). Because large floods in two seasons were found to complicate the LCR-associated results, the three sediment years with large LCR floods in two seasons (i.e., 2008, 2010, and 2017) were excluded from the analyses utilizing LCR data.

3.5. Sand Budgets

Continuous mass-balance sand budgets were constructed for the UMC, LMC, EGC, ECGC, and WCGC segments of the Colorado River (Figure 1) using the sand-load data described in Section 3.1. For the 2002–2007 period when sand-transport measurements were not made at the RK268 station, the ECGC and WCGC segments were treated as a single Central Grand Canyon (CGC) segment. Over a given time interval in each segment,

$$\Delta S = I + I_{\mathrm{T}} + I_{\mathrm{LT}} - E \tag{5}$$

where ΔS is the sand mass balance, I is the measured sand load (input) at the upstream station, I_T is the measured sand load of the major tributaries, I_{LT} is the measured/estimated sand load of the lesser tributaries, and E is the measured sand load (export) at the downstream station. The only two major tributaries are the Paria River and LCR, which respectively supply sand to UMC and EGC. The sand loads of Kanab and Havasu creeks (the only other larger tributaries) are included in the estimated ECGC lesser-tributary sand loads (Text S5). We set $I = 0$ for UMC because sand loads at the RK0 station are generally negligible, that is, much smaller than the uncertainties in I_T and I_{LT} for UMC (e.g., Topping et al., 2010).

Uncertainties in ΔS are calculated by propagating the load uncertainties described in Section 3.1 through Equation 5. Because these uncertainties are expressed as relative values, the uncertainties accumulate over time when expressed as absolute magnitudes. ΔS is deemed indeterminate when the uncertainty is ≥ 1.5 times the absolute value of the zero-bias value; ΔS is demonstrably positive or negative when the uncertainty is < the absolute value of the zero-bias value; and ΔS is likely positive or negative when the uncertainty falls between these bounds. Because the uncertainty in ΔS arises from possible persistent biases in the loads, the distribution of the uncertainty is unknown, but is likely between uniform and normal. When the uncertainty is 1 or 1.5 times the absolute value of the zero-bias value, respectively, 100% or 83% of the uncertainty band about the zero-bias value lies either above or below $\Delta S = 0$. If the uncertainty is uniformly distributed, the 1.5 value we use thus yields an 83% confidence interval. Under the more likely possibility that the uncertainty distribution is closer to normal than uniform, the 1.5 value yields a confidence interval similar to the 95% confidence interval we use for our other analyses.

The accuracy of our flux-based sand budgets was evaluated through two independent comparisons with topographic-based sand budgets (Grams et al., 2019; Kaplinski et al., 2020a, 2020b). These topographic sand budgets were constructed using bathymetric and topographic measurements made 3 years apart covering ∼71% of LMC and ∼50% of EGC.

4. Results

4.1. Tributary Sand Supply

The tributary fine-sediment (i.e., sand, silt, and clay) supply to the Colorado River in our study area is bimodal, with a clay primary mode and a sand-silt secondary mode (Text S9). The tributary sand supply grades smoothly into the silt-and-clay supply such that the sand-size sediment comprises the coarser part of this secondary mode, which occurs in very fine sand (0.0625–0.125 mm) for the Paria River and in medium silt (0.0156–0.0312 mm) for the LCR. Both tributaries supply more silt and clay to the Colorado River than they do sand. During sediment years 1998–2017, silt and clay comprised 60.6% and 88.1% of the fine sediment supplied by the Paria River and LCR, respectively.

The flashy nature of the tributaries causes their sediment supply to be highly episodic. During sediment years 1998–2017, the Paria River was the largest sand supplier, with a mean-annual sand load of 890,000 ± 89,000 Mg, and the LCR was the second-largest sand supplier, with a mean-annual sand load of 580,000 ± 58,000 Mg (Figure 2). These values are substantially less than those estimated by Topping, Rubin, and Vierra (2000). Although none of the other tributaries are substantial suppliers of sand (Text S6), since July 2011 they have collectively supplied a sand amount equivalent to that of the LCR. Of the total amount of sand supplied since 2011, the Paria River has contributed 57%, the LCR has contributed 21%, and all other tributaries combined have contributed 22% (a value slightly less than the lowest-bound estimate of Webb et al., 2000). The largest quantities of sand are supplied by the Paria River and LCR during summer thunderstorm-generated floods that last hours to a day. As the result of the hydrologically flashy nature of these tributaries, half of the 1998–2017 Paria River and LCR sand supplies were delivered to the Colorado River over only 26 and 27 days, respectively (i.e., 0.4% of all days).

Owing to this highly episodic behavior, sand loads in the Paria River and LCR are uncorrelated on a daily basis ($r = 0.13$) and only weakly correlated on a monthly basis ($r = 0.27$). This result provides justification for the lagged-covariance analysis in Section 3.4 to be conducted independently for these two rivers, neglecting the influence over shorter timescales of the other tributary on the bed sand in Grand Canyon (downstream from both tributaries). The highly episodic nature of large sand loads leads to the distributions of the Paria River and LCR loads during individual months being mostly right-skewed. Thus, the median
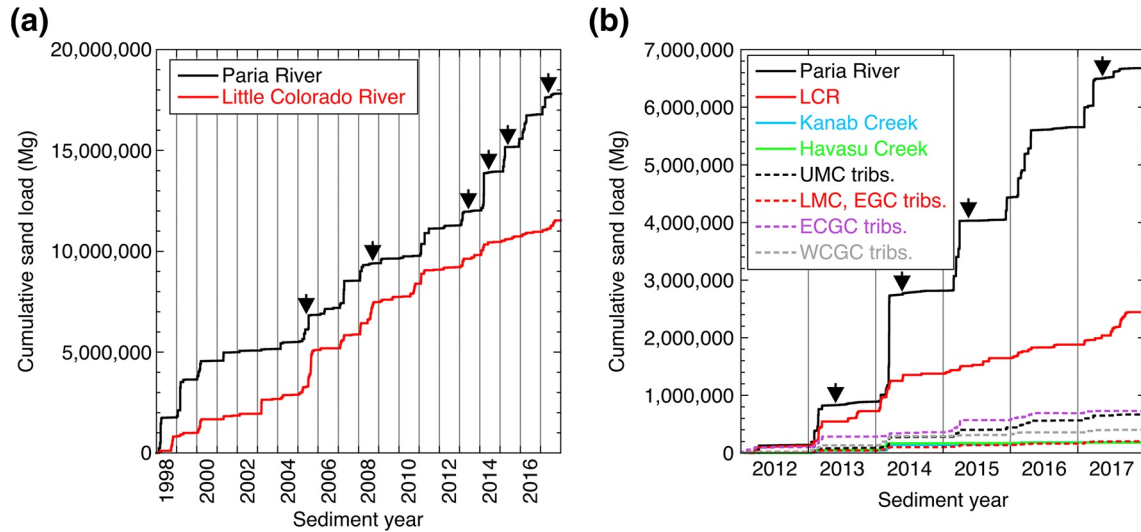
Figure 2. Cumulative tributary sand loads. (a) Cumulative measured sand loads of the Paria River and LCR over the entire period of our study. (b) Sediment year 2012–2017 cumulative measured sand loads of the Paria River, LCR, Kanab Creek (at the Kanab Creek–mouth station), and Havasu Creek, and cumulative estimated sand loads of the lesser tributaries in each segment. EGC lesser-tributary loads were estimated as equivalent to LMC lesser-tributary loads. For the comparison in (b), the cumulative measured sand loads of Kanab and Havasu creeks were removed from the estimated sand load of the ECGC lesser tributaries. The cumulative sand load of Kanab Creek is almost completely hidden behind that of Havasu Creek in (b). Black arrows indicate times of controlled floods. ECGC, East-Central Grand Canyon; EGC, Eastern Grand Canyon; LCR, Little Colorado River; LMC, Lower Marble Canyon; WCGC, West-Central Grand Canyon.

sand load is a better indicator of the central tendency of the distribution of monthly loads than the mean. For example, the maximum January sand load of the Paria River was 660,000 Mg, whereas the January mean and median sand loads were respectively 43,000 and 2,000 Mg. Large sand loads are rare during winter and spring months on both rivers, as illustrated by the large disparity between the median and maximum values (Figure 3).

The tributary sand supply is generally much finer than the Colorado River bed sand, such that the typical D_{50} of the bed sand greatly exceeds the D_{84} of the tributary sand supply. The D_{16}, D_{50}, and D_{84} of the Q_{SAND}-weighted grain-size distribution of the sand supplied by the Paria River are 0.079, 0.127, and 0.237 mm, respectively, and for the LCR are 0.076, 0.121, and 0.228 mm, respectively (Text S9). In addition, the grain-size distributions of the sand supplied by these tributaries are highly right-skewed such that roughly equivalent large amounts of sand are
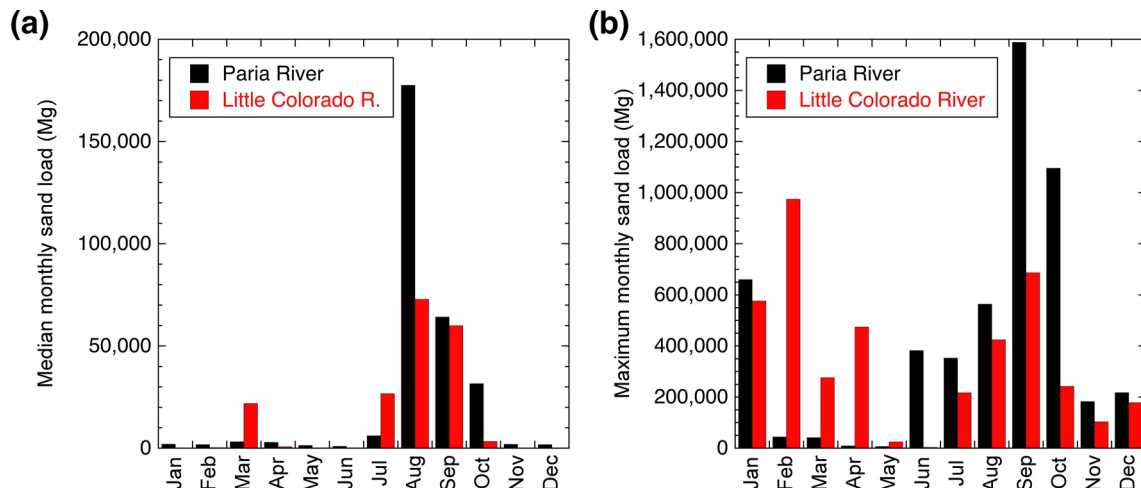

Figure 3. (a) Median and (b) maximum measured sand loads of the Paria River and Little Colorado River (LCR) for each month during sediment years 1998–2017.

present in each of the ¼-ϕ size classes between the 0.0625-mm silt bound and the D_{50} value. Grain-size analyses of suspended-sediment measurements in other tributaries indicate that the sand supplied by these other tributaries is generally as fine or finer than the Paria River and LCR sand. Mean values of the cross-sectionally averaged bed-sand D_{50} (i.e., D_{B-REF}) at the RK49, RK99, RK141, RK268, and RK363 stations on the Colorado River are respectively 0.34, 0.34, 0.39, 0.36, and 0.36 mm (Text S7).

4.2. Regulation of Suspended-Sand Concentration by Flow and Grain Size

Graphical analyses of the suspended-sand datasets at all six stations on the Colorado River indicate a hybrid behavior between strictly flow- and grain-size-regulated scenarios (Figure 4, Text S4). Although C_{SAND} generally increases with increasing Q, variance in the relations between Q and C_{SAND} is large, systematic, and associated with D_S. Consequently, the largest values of C_{SAND} are not necessarily associated with the largest values of Q but are instead typically associated with the smallest values of D_S (Text S4). Although the slopes of the relations between Q and D_S tend to be positive (as expected in the flow-regulated scenario), the variance about these relations is very large and the largest values of D_S generally occur at lower values of Q (the opposite of what occurs in the flow-regulated scenario). Regressions of $\log_{10}(C_{SAND})$ on $\log_{10}(D_S)$ over small Q increments indicate that most Q-independent variation in C_{SAND} can be explained by a change in bed-sand grain size at the 95% confidence interval (Text S4). The average maximum Q-independent variation in C_{SAND} not attributable to grain size is only a factor of ~6–8. This small magnitude of variation is well within that plausibly caused by the ranges in reach-averaged bed-sand area and τ_B described in Section 1.2 (cf. Rubin et al., 2020).

α analyses confirm the hybrid flow- and grain-size regulation of C_{SAND} suggested by the graphical analyses of Q, C_{SAND}, and D_S (Table 1). Although variation exists in $|\alpha|$ between stations, F-tests indicate that no significant longitudinal trends exist in $|\alpha|$ among each measurement type ($p > 0.05$). On the basis of the EDI/EWI/VPA and calibrated-pump measurements, Q is roughly two to four times as important as bed-sand grain size in regulating C_{SAND}. In contrast, on the basis of the less-accurate but more continuous 15-min acoustical measurements, bed-sand grain size is as or slightly more important than Q in regulating C_{SAND}. The most accurate $|\alpha|$ values are obtained when the suspended-sand data used to calculate $|\alpha|$ include all C_{SAND} and D_S conditions at each Q, in the proportions that these conditions occur. Although only the 15-min acoustical data meet this criterion, they may not result in the most accurate $|\alpha|$ values because the acoustical measurements are the least accurate of the suspended-sand measurements used in our study. The acoustical measurements exhibit a broader range in D_S at low Q than do the other measurement types (Text S4), and these values contribute to higher $|\alpha|$. Thus, bed-sand grain size likely plays an important secondary role in regulating C_{SAND} but does not generally dominate over the regulation of C_{SAND} by Q in the Colorado River.

4.3. β, Bed-Sand Grain Size, and the Dependence of Bed-Sand Grain Size on Discharge

Changes in β track direct measurements of the bed-sand grain-size distribution in the Colorado River, albeit with large variance (Text S10). The values of β calculated from the EDI/EWI/VPA suspended-sediment measurements are significantly correlated with the bed-sand coarseness in the measurement cross-sections at all stations where direct bed-sediment measurements were made. Except at the RK99 station, the positive correlations between β and D_B are weak ($r = 0.3$–0.4), and the negative correlations between β and $\log_{10}(f_{VF})$ are moderate to strong ($r = -0.4$ to -0.8). This result, where β is better correlated with the fractional amount of very fine sand than it is with D_B, is identical to the result from longitudinal sampling in 1999 (Text S2) and is the expected result when the D_B Rouse number is >1 (Topping et al., 2018).

The strength of the correlation between β and the direct measurements of bed-sand grain size provides a measure of how the bed-sand grain size at a single cross-section reflects the spatially averaged bed-sand grain size over the reach scale. Stronger correlations between β and either D_B or $\log_{10}(f_{VF})$ indicate that the bed-sand conditions at the measurement cross section are representative of the spatially averaged bed-sand conditions in the upstream reach and imply that the bed-sand grain-size distribution may be relatively uniform over the reach scale. Given the moderate to strong correlations between β and $\log_{10}(f_{VF})$, roughly 20% to 60% of the variance in bed-sand grain size at a single cross section is not explained by β. This unexplained variance does not arise from error because its magnitude (Figure 1 in Text S10) greatly exceeds the ±10% 95%-confidence-level relative error
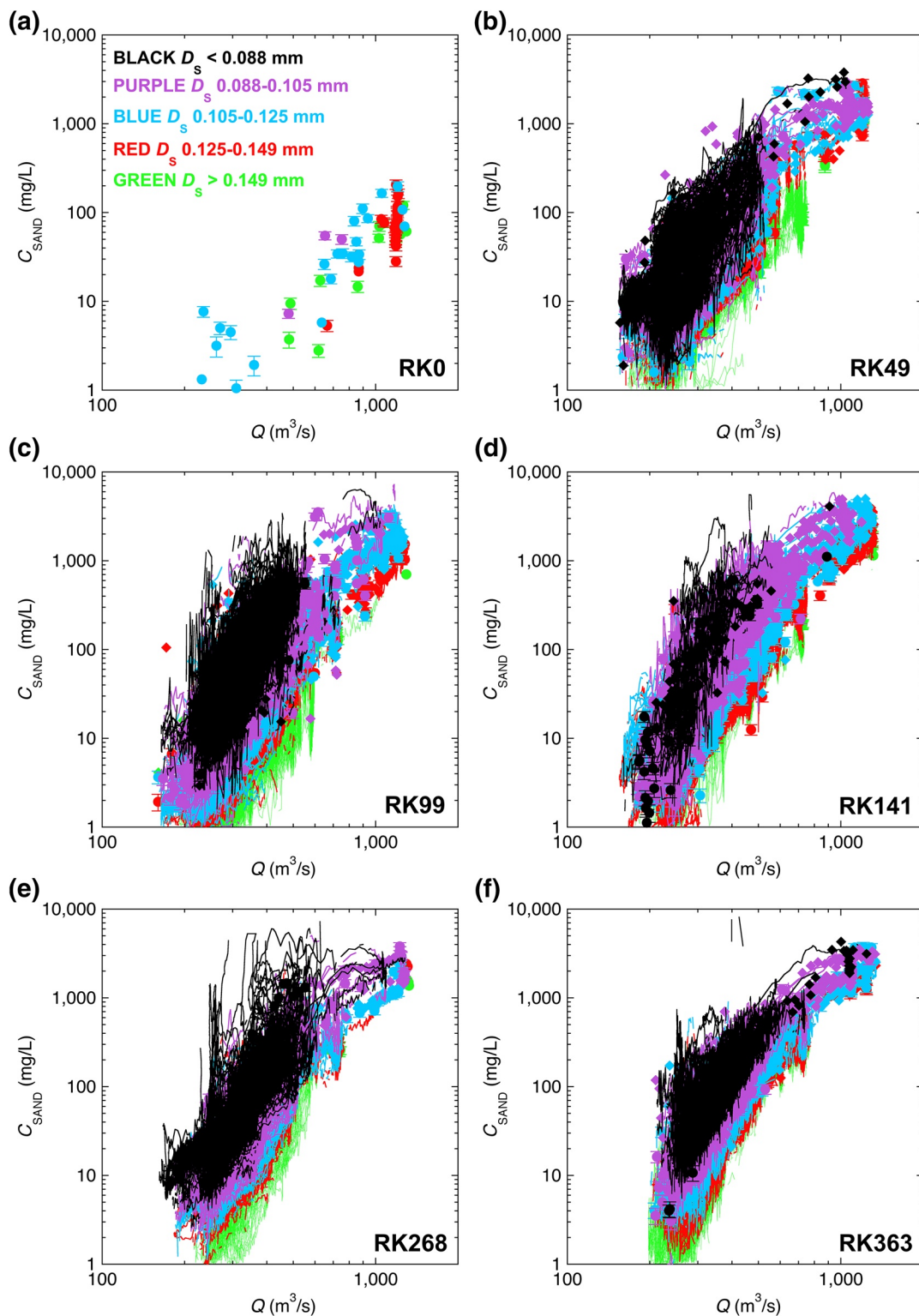
Figure 4. Velocity-weighted suspended-sand concentration in the river cross section (C_{SAND}) plotted as a function of instantaneous water discharge (Q) segregated by D_S and measurement type at the (a) RK0, (b) RK49, (c) RK99, (d) RK141, (e) RK268, and (f) RK363 stations. D_S is used to segregate associated values of C_{SAND} into five grain-size bins; bin colors indicated in panel (a). 15-min acoustical measurements connected by line segments (breaks in line segments occur when C_{SAND} transitions between bins), calibrated-pump measurements plotted as diamonds, EDI/EWI/VPA measurements plotted as circles. Error bars on EDI/EWI measurements indicate 95%-confidence-level combined field and laboratory errors. Error bars on calibrated-pump and acoustical measurements not shown to avoid clutter. At any given Q, higher C_{SAND} is typically associated with finer D_S, and therefore finer bed sand. EDI, Equal-Discharge-Increment; EWI, Equal-Width-Increment; VPA, Velocity-weighted-average Point-sample Array.

Table 1
Results From α Analyses

Station	Measurement type	Sediment years	n	$|\alpha|$
RK0	EDI	1996–2017	69	0.43
RK49	Multifrequency acoustical	2008–2017	322,449	1.5
	Calibrated pump	2003–2017	1,760	0.35
	EWI/VPA	2001–2017	423	0.36
RK99	Multifrequency acoustical	2007–2017	314,549	1.4
	Calibrated pump	2003–2017	1,752	0.23
	EWI/EDI/VPA	1996–2017	957	0.21
RK141	Multifrequency acoustical	2005–2017	415,006	0.39
	Calibrated pump	2002–2017	2,223	0.38
	EDI/EWI/VPA	1996–2017	1,884	0.33
RK268	Multifrequency acoustical	2008–2017	320,084	0.92
	Calibrated pump	2008–2013	171	0.19
	EWI/VPA	1996–2017	277	0.37
RK363	Multifrequency acoustical	2008–2017	308,428	0.87
	Calibrated pump	2003–2017	1,952	0.29
	EDI/EWI/VPA	1998–2017	392	0.25

Note. n indicates the number of suspended-sand measurements in each analysis.

EDI, Equal-Discharge-Increment; EWI, Equal-Width-Increment; VPA, Velocity-weighted-average Point-sample Array.

in the EDI/EWI/VPA-calculated β values. Rather, this unexplained variance must arise from real differences between the reach-averaged bed-sand grain size and the bed-sand grain size at only one cross section. The result that the amount of variance in bed-sand grain size unexplained by β is much larger in the Colorado River (i.e., 20%–60%) than in flume experiments (i.e., <4%) is not unexpected. D_B and f_{VF} in Einstein and Chien's (1953b) flume experiments were calculated from spatially averaged bed-surface measurements. Conversely, D_B and f_{VF} in the Colorado River were calculated from direct bed-sediment measurements at only a single cross section. By definition, β is a measure of the spatially averaged bed-sand grain size in the reach upstream from this cross-section.

Bed-sand grain size is generally negatively correlated with Q in the Colorado River on the basis of both β and direct bed-sediment measurements (Figure 2 in Text S10). Thus, the bed-sand fining observed during the rising limb of controlled floods (Topping et al., 2010, 1999) occurs during most increases in Q. Moreover, this result indicates that the bed sand in the channel does actually fine with increasing Q, and the negative correlation between β and Q does not arise from the suspended sand merely interacting with higher-elevation finer sand deposits inundated only at higher Q. Therefore, increases in Q cause both an increase in bed-sand area (Section 1.2) and a decrease in bed-sand grain size. Because we sought to investigate the physical linkages between sand-wave-migration, bed-sand grain size, and sand storage, and not the transient response of bed-sand grain size to Q, we detrended β as a function of Q using the relations in Text S10. We refer to Q-detrended β as β_Q.

4.4. Migration of Sand Waves Downstream from Tributaries

Our late-1990s observations suggested that tributary floods generated sand waves that split into two packets, A and B (Section 1.2): packet A was finer than packet B and migrated downstream in the Colorado River with a celerity slightly slower than the water velocity (Topping, Rubin, Nelson et al., 2000). The arrival of the front of packet A caused large preferential increases in the finest size classes of sand in the bed and in suspension, such that the peak of packet A was associated with minima in β and D_B and a maximum in f_{VF} (Text S2). Net sand deposition occurred as packet A migrated downstream; between RK31–36 and the RK99 station, the amount of sand transported in packet A was observed to decrease from ∼20%–30% to <10% of the amount supplied during its source Paria River flood. Packet B migrated much more slowly than packet A; the amalgamated front of packet B had migrated only ∼10 km in the 3 and 10 days after two Paria River floods (Topping, Rubin, Nelson et al., 2000; Text S2). Though the arrival of packets A and B caused bed-sand fining, the fining caused by packet A was restricted to increases in very fine (0.0625–0.125 mm) sand whereas the fining caused by packet B occurred through increases in the very fine through fine (0.0625–0.25 mm) sand. Because β is most sensitive to changes in the amount of the finest sand on the bed, the peak of packet A is thus expected to present as the primary peak in the cross covariance of tributary Q_{SAND} and Colorado River $1/\beta_Q$ (hereafter abbreviated as Q_{SAND}—$1/\beta_Q$ cross covariance).

Lagged-covariance analyses confirm that the 1990s-observed splitting of tributary-generated sand waves into two packets is a general characteristic of the sand waves in the Colorado River (Figure 5). The leading part of a sand wave presents as the primary peak in Q_{SAND}—$1/\beta_Q$ cross covariance and migrates downstream in the Colorado River at a velocity slightly slower than that of the peak of the silt-and-clay wave (Text S8), which, in turn travels downstream at a velocity slightly slower than that of the water (Figure 6). The second, trailing, part of a sand wave has lower celerity and presents as a secondary, broader cross-covariance peak. This style of sand-wave migration is consistent with the primary cross-covariance peak reflecting the grain-size minimum caused by the maximum in f_{VF} at the peak of packet A, and the secondary cross-covariance peak reflecting the minimum in D_B at the peak of packet B. Inspection of the 15-min data used in the lagged-covariance analyses indicates that the longitudinal
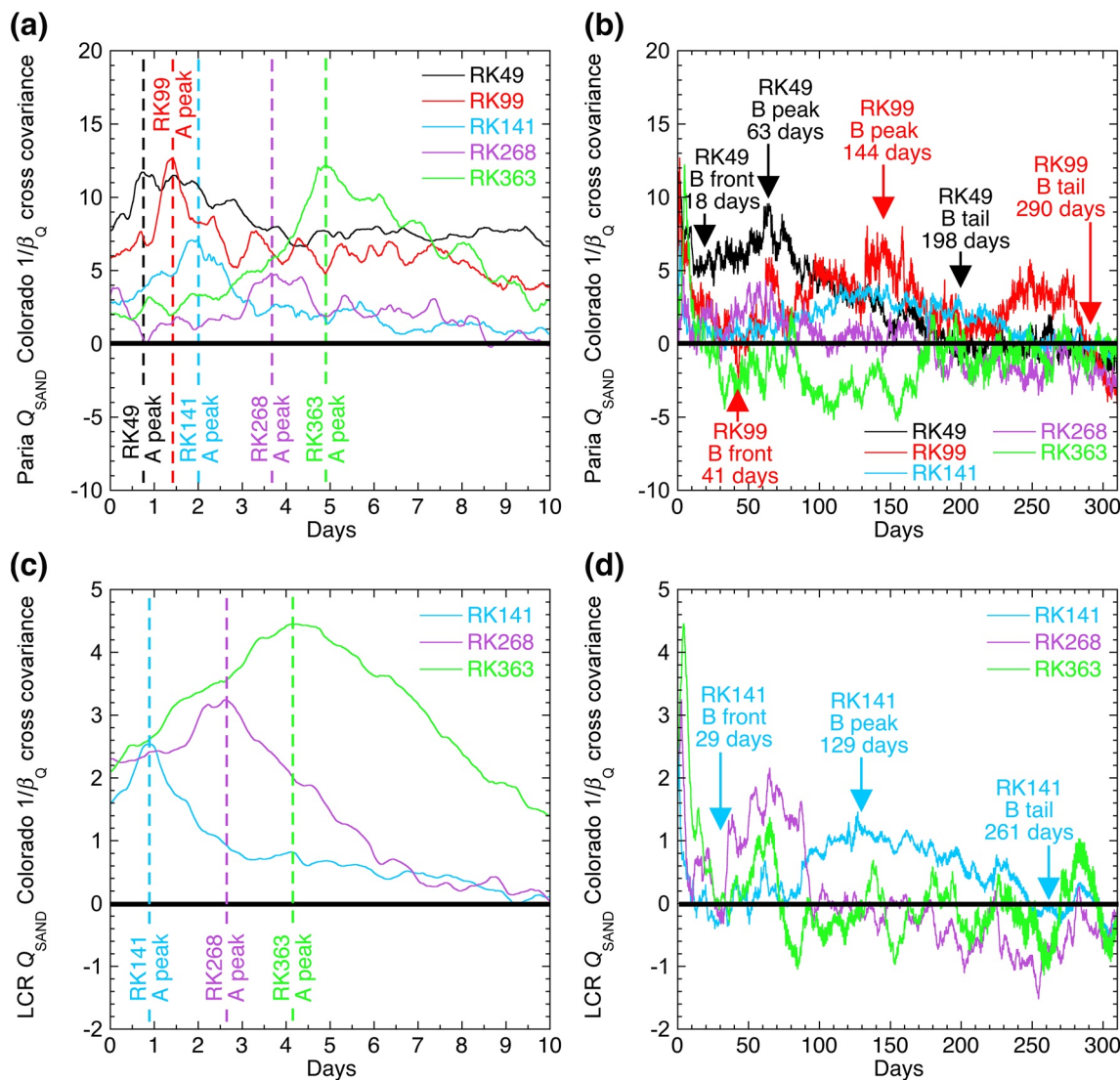
Figure 5. (a) and (b) Paria Q_{SAND}—Colorado $1/\beta_Q$ cross covariance and (c) and (d) LCR Q_{SAND}—Colorado $1/\beta_Q$ cross-covariance plotted as a function of time. (a) and (c) are expanded views of the first 10 days in (b) and (d), showing the times of the primary cross-covariance peaks associated with packet A. The times of the front, peak value, and tail of the secondary cross-covariance peaks associated with packet B are indicated in (b) and (d); these times were identified by fitting a smoothed curve (Text S8). Though Q_{SAND}—$1/\beta_Q$ cross covariance has cross-section-integrated mass-flux units of kg/s because β_Q is nondimensional, differences in cross covariance among the Paria River or LCR cases reflect relative differences in bed-sand grain size (Text S8). The broad secondary peak at the RK141 station in (b) is likely not associated with Paria-River-generated sand waves (Text S8). LCR, Little Colorado River.

differences in the magnitudes of the primary cross-covariance peaks in Figure 6 arise from the times and shapes of the $1/\beta_Q$ peaks following Paria River and LCR floods being more irregular at the RK141 and RK268 stations than at the other stations.

The primary peak in Q_{SAND}—$1/\beta_Q$ cross covariance decays to background within 7–20 days of a tributary flood at all but the RK49 station, thus indicating that much of packet A exits our study area quickly (Figure 5). The primary cross-covariance peak occurs at the RK363 stations 4.9 days after a 15-min period of large Q_{SAND} in the Paria River and 4.1 days after a 15-min period of large Q_{SAND} in the LCR (Figures 5a and 5c). Among the 10 days of largest sand load in these tributaries during 2008–2017, ~7% and ~27% of the sand respectively supplied by the Paria River and LCR were transported past the RK363 station within the peak of packet A five through 7 days later (i.e., days 4.0 through 7.0 in Figure 5). These amounts are consistent with our late-1990s observations and provide a crude estimate of the tributary-supplied sand exported from our study area quickly in packet A. More-
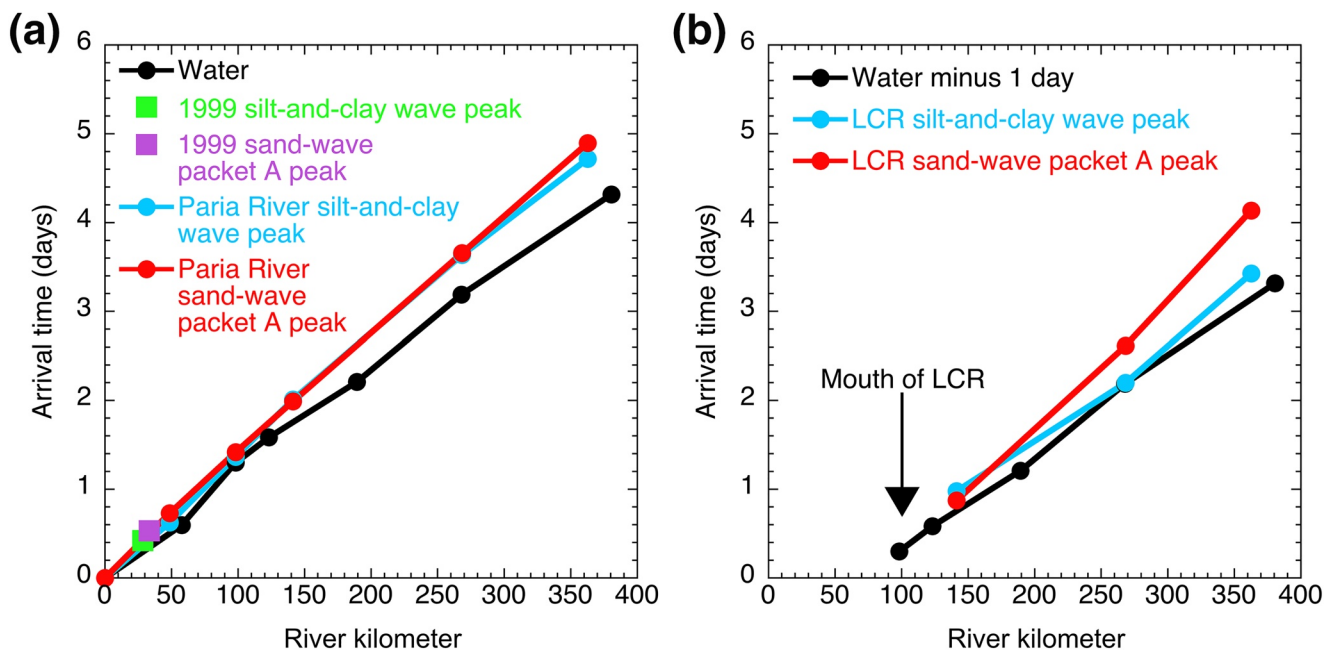
Figure 6. Arrival times of water, the peak of the silt-and-clay wave, and the peak of sand-wave packet A generated during (a) Paria River and (b) LCR floods. Water arrival times from dye measurements of Graf (1995). Ancillary background information for this figure is in Text S8. LCR, Little Colorado River.

over, the respective Q_{SAND}-weighted mean values of D_S at the RK363 station during these ten 3-day periods were 0.091 and 0.085 mm, values equivalent to the D_{25} and D_{23} of the sand supplied by the Paria River and LCR. Thus, the amount of very fine sand exported to Lake Mead within a week of a large tributary flood is nonnegligible, with perhaps a larger fraction of LCR-supplied sand never retained in the Colorado River (cf. Topping, Rubin, Nelson et al., 2000).

The lower celerity of packet B causes the secondary cross-covariance peak to become distinct from the primary peak with increasing distance downstream. Following a Paria River flood, the secondary peak (packet B) separates from the primary peak (packet A) between the RK49 and RK99 stations, and it takes ~198 and ~290 days for the tail of packet B to respectively reach these stations. Following an LCR flood, packet B separates from packet A upstream from the RK141 station, and it takes ~261 days for the tail of packet B to reach this station. The amplitude of the secondary cross-covariance peak associated with packet B decays in the downstream direction (Figures 5b and 5d), such that this peak cannot be detected at stations most distal to the flooding tributary. Although sand-wave dispersion (Cui, Parker, Lisle et al., 2003; Cui, Parker, Pizzuto et al., 2003; Lisle, 2007) likely contributes to this result, this result may also arise from packet B's celerity becoming more irregular as it migrates downstream. By this process, the amplitude of packet B does not decay, but rather the time that packet B's peak passes a given Colorado River station becomes less systematic with greater migrated distance. If dispersion were the only cause of the downstream decay in the amplitude of the secondary cross-covariance peak, $|\alpha|$, the grain-size-associated variation in C_{SAND}, and the variation in bed-sand grain size (Section 4.5) would all systematically decrease in the downstream direction. As shown in Section 4.2, $|\alpha|$ among each measurement type does not systematically change in the downstream direction, nor does the grain-size-associated variation in C_{SAND}.

4.5. Time Series of Bed-Sand Grain Size

Despite the presence of the large-scale variation in bed-sand grain size caused by the sand-wave migration documented in the previous section, relatively little net change in bed-sand grain size has occurred in the Colorado River over the period of our study (Figure 7). Moreover, variation in bed-sand grain size does not systematically decrease in the downstream direction; for each measurement type, F-tests indicate no significant longitudinal trend in the standard deviation in β_Q among the stations ($p > 0.05$). Although the β_Q values

calculated from the acoustical and calibrated-pump measurements captured more of the shorter-term variability in bed-sand grain size than did the β_Q values calculated from the sparser EDI/EWI/VPA measurements, we analyzed trends in the β_Q values calculated from the EDI/EWI/VPA measurements, which spanned a much longer period. Whereas no significant long-term trend in β_Q was detected at the RK0, RK49, and RK99 stations (Figures 7a–7c), β_Q decreased significantly at the RK141 (by ~21%), RK268 (by ~16%), and RK363 (by ~14%) stations (Figures 7d–7f). These results suggest that, between 1996 and 2017, little net change in bed-sand grain size occurred in Lower Glen Canyon and in Marble Canyon, whereas bed-sand fining occurred farther downstream in Grand Canyon. These long-term trends in β_Q-inferred reach-averaged bed-sand grain size are generally supported by similar long-term trends in D_B and f_{VF} from the single-cross-section direct bed-sediment measurements (Text S11).

4.6. Continuous Mass-Balance Sand Budgets

Comparison of our flux-based continuous mass-balance sand budgets with topographic-based sand budgets indicates that the mass-balance budgets are accurate at our specified level of uncertainty. Repeat mapping indicates that 640,000 ± 350,000 Mg of sand were eroded from LMC between May 2009 and May 2012 (Grams et al., 2019). This measurement includes extrapolation of the measured change in sand mass to the unmapped part of this segment; uncertainty is the 95%-confidence-level error. During this same period, our flux-based sand budget indicates that 690,000 ± 320,000 Mg of sand were eroded from LMC. In EGC, repeat mapping indicates that 630,000 ± 480,000 Mg of sand were eroded between April 2011 and May 2014 (Text S12; Kaplinski et al., 2020a; Kaplinski et al., 2020b), whereas our flux-based sand budget indicates 740,000 ± 610,000 Mg of sand erosion. These results from two independent comparisons (i.e., different river segments and time periods) indicate that our continuous mass-balance sand budgets are sufficiently accurate for the analyses herein.

The magnitude of accumulating uncertainty was large enough relative to the sand mass balance (ΔS) such that ΔS could not be known in any of the five segments over the entire period of our study (Figure 8, Table 2). Unattainably low uncertainties <5% for I and E, and <10% for I_T would be required to know ΔS over decade-plus timescales. Although ΔS remained uncertain over long timescales owing to small differences between large values of I or I_T and E, the uncertainty was small enough that ΔS was rarely indeterminate over shorter timescales. ΔS generally had demonstrable sign in all segments over annual timescales (>77% of all 69 segment-years), and almost always had demonstrable sign over monthly timescales (>90% of all 833 segment-months). Segregation of the Colorado River into the five UMC, LMC, EGC, ECGC, and WCGC segments allowed better determination of the loci of erosion and deposition without universally increasing the occurrence of years with indeterminate ΔS (Table 2). The use of only two segments, one for Marble Canyon and one for Grand Canyon, reduced the number of indeterminate ΔS years in only Marble Canyon.

4.7. Relations Between Sand Storage and Bed-Sand Grain Size

The total amount of sand stored in the Colorado River in our study area should be negatively correlated with bed-sand grain size because the tributary sand supply is generally much finer than the bed sand in the Colorado River. At any given time, the total mass of sand stored in a segment is equal to the cumulative ΔS plus an unknown constant that accounts for the "background" sand storage that existed when monitoring began. As in Figure 8, "cumulative ΔS" is the sand mass balance calculated relative to a zero value at the time when continuous suspended-sediment monitoring began at the stations bracketing that segment. We therefore evaluated whether we could detect the expected negative relation between reach-averaged bed-sand grain size and cumulative ΔS (i.e., the proxy for the total amount of sand storage) using β_Q calculated from the continuous acoustical data (Table 3). For these analyses, we used the 15-min β_Q values at the upstream and downstream stations bracketing each segment as well as the average β_Q of these values.

Although cumulative ΔS is universally negatively correlated with β_Q at the upstream station and with β_Q averaged between the upstream and downstream stations, cumulative ΔS is negatively correlated with downstream β_Q in only 60% of all cases. The lesser-tributary sand supply is negligible compared to the upstream sand supply in each segment, thus almost all of the sand supplied to a segment passes the upstream station. Consequently,
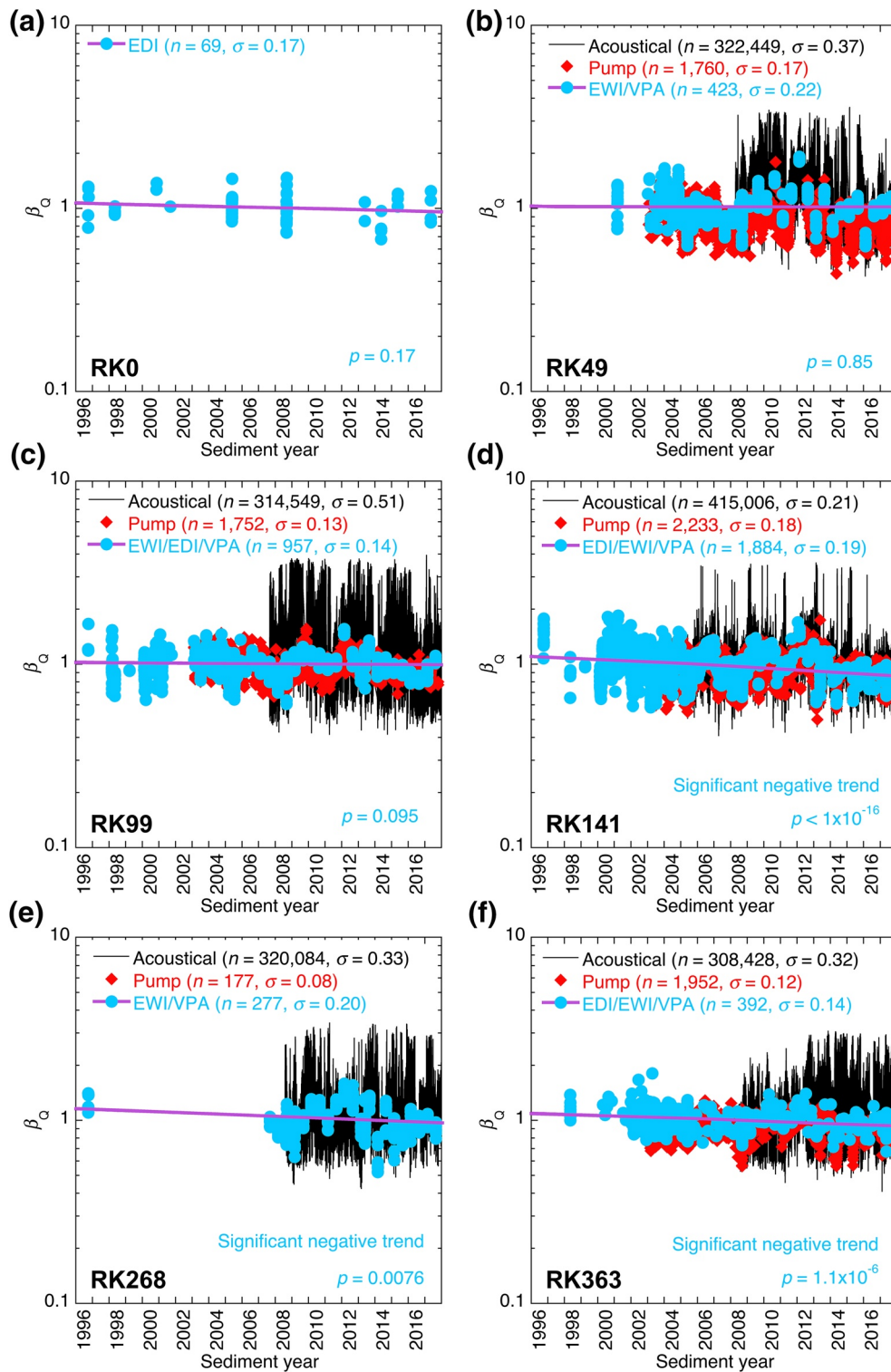
Figure 7. β_Q plotted as a function of time at the (a) RK0, (b) RK49, (c) RK99, (d) RK141, (e) RK268, and (f) RK363 stations. β_Q values calculated from the acoustical, calibrated-pump, and EDI/EWI/VPA suspended-sand measurements plotted separately, with number of measurements (n) and standard deviation (σ) in β_Q indicated. Pump measurements at the RK268 station were made only during controlled floods; RK268 pump-measurement β_Q values are thus hidden behind EWI/VPA β_Q values. Least-squares linear regressions (purple lines) fit to β_Q calculated from the EDI/EWI/VPA measurements, with associated levels of significance (p) shown. EDI, Equal-Discharge-Increment; EWI, Equal-Width-Increment; VPA, Velocity-weighted-average Point-sample Array.
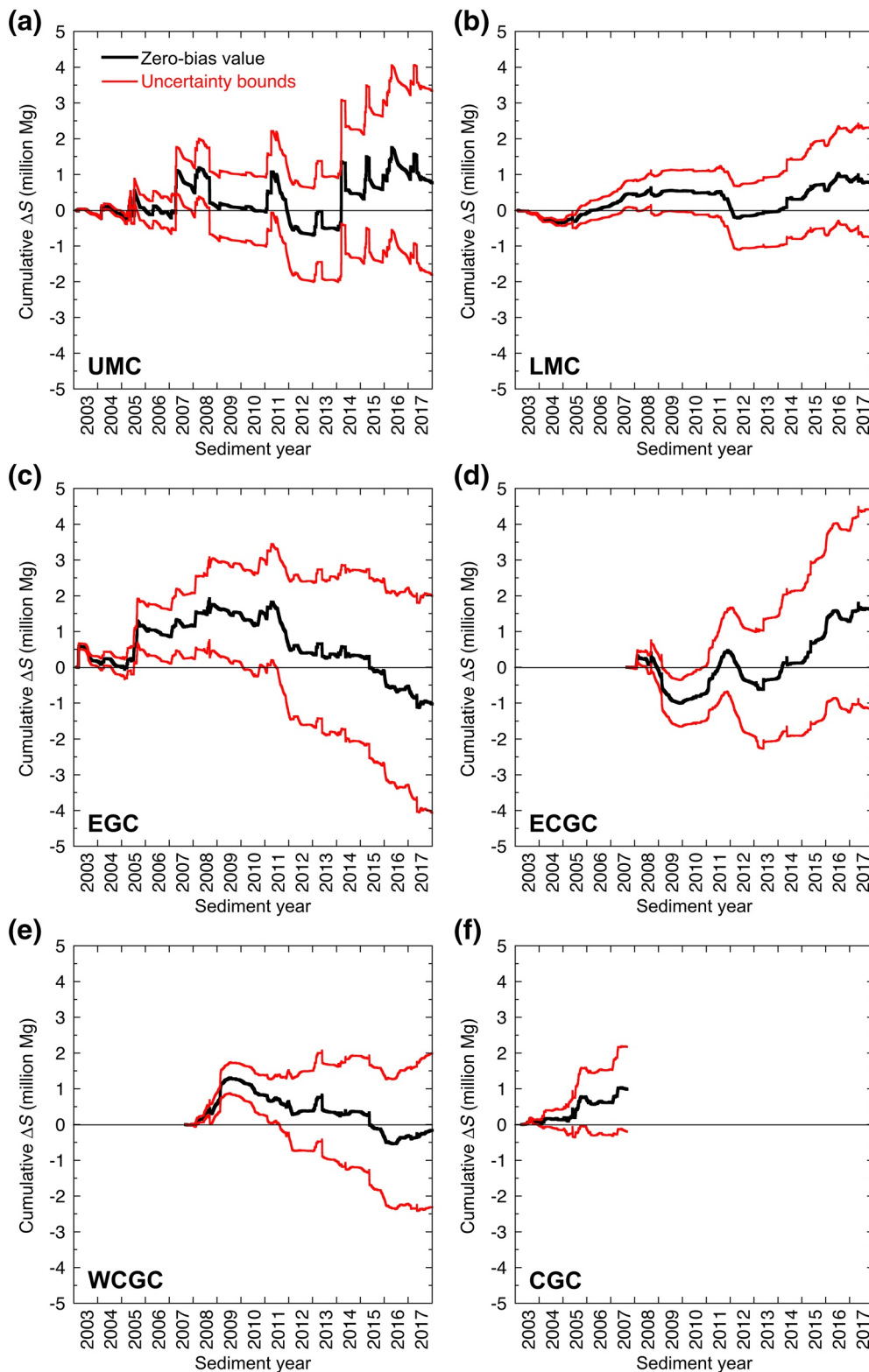
Figure 8. Continuous mass-balance sand budgets for the (a) UMC, (b) LMC, (c) EGC, (d) ECGC, (e) WCGC, and (f) CGC segments. Cumulative ΔS in this figure is the sand mass balance calculated relative to a zero value at the time when continuous suspended-sediment monitoring began at the stations bracketing that segment. The total amount of sand stored in a segment at any given time equals cumulative ΔS plus an unknown constant for the sand already in storage in that segment when monitoring began. CGC, Central Grand Canyon; ECGC, East-Central Grand Canyon; EGC, Eastern Grand Canyon; LMC, Lower Marble Canyon; UMC, Upper Marble Canyon; WCGC, West-Central Grand Canyon.

Table 2
Annual Sand-Budget Results With Propagated Uncertainties

Sediment year	RK0 annual mean Q (m^3/s)	Paria River annual sand load (million Mg)	LCR annual sand load (million Mg)	ΔS in UMC segment (million Mg)	ΔS in LMC segment (million Mg)	ΔS in Marble Canyon (million Mg)	ΔS in EGC segment (million Mg)	ΔS in ECGC segment (million Mg)	ΔS in WCGC segment (million Mg)	ΔS in Grand Canyon[a] (million Mg)
2003[b]	326	0.0081	0.73	−0.15 ± 0.024	−0.18 ± 0.035	−0.33 ± 0.036	**0.16 ± 0.14**			
2004	326	0.34	0.21	*0.031 ± 0.068*	−0.17 ± 0.048	−0.14 ± 0.081	−0.16 ± 0.097		*0.091 ± 0.21*[c]	−0.067 ± 0.22
2005	329	1.3	2.2	*0.11 ± 0.27*	**0.28 ± 0.17**	**0.39 ± 0.30**	**1.1 ± 0.44**	**0.55 ± 0.54**[c]	0.55 ± 0.54 [c]	**1.6 ± 0.74**
2006	332	0.34	0.079	−0.14 ± 0.077	**0.21 ± 0.049**	**0.077 ± 0.075**	−0.22 ± 0.063	−0.066 ± 0.088[c]	−0.066 ± 0.088[c]	−0.28 ± 0.088
2007	330	1.3	0.70	**0.69 ± 0.24**	**0.31 ± 0.089**	**1.0 ± 0.25**	**0.30 ± 0.17**	**0.34 ± 0.29**[c]	0.34 ± 0.29[c]	**0.64 ± 0.36**
2008	346	0.87	1.6	−0.45 ± 0.20	*−0.023 ± 0.16*	−0.47 ± 0.22	**0.51 ± 0.38**	−0.068 ± 0.40	**0.59 ± 0.28**	**1.0 ± 0.52**
2009	339	0.24	0.26	−0.032 ± 0.050	**0.11 ± 0.028**	**0.076 ± 0.049**	−0.19 ± 0.072	−0.90 ± 0.23	**0.65 ± 0.16**	−0.45 ± 0.22
2010	334	0.13	0.66	−0.090 ± 0.032	−0.047 ± 0.030	−0.14 ± 0.038	*0.0063 ± 0.13*	**0.26 ± 0.10**	−0.41 ± 0.096	−0.14 ± 0.16
2011	427	1.4	0.69	−0.19 ± 0.29	−0.40 ± 0.21	−0.59 ± 0.33	−0.90 ± 0.38	**1.1 ± 0.48**	−0.20 ± 0.32	−0.045 ± 0.52
2012	441	0.14	0.12	−0.47 ± 0.052	−0.23 ± 0.083	−0.70 ± 0.073	−0.21 ± 0.13	−0.87 ± 0.22	−0.24 ± 0.24	−1.3 ± 0.25
2013	319	0.75	0.60	**0.16 ± 0.15**	**0.11 ± 0.075**	**0.27 ± 0.15**	−0.063 ± 0.17	0.16 ± 0.26	−0.072 ± 0.21	−0.020 ± 0.38
2014	297	1.9	0.65	**0.97 ± 0.35**	**0.34 ± 0.13**	**1.3 ± 0.36**	*−0.00073 ± 0.22*	**0.42 ± 0.30**	0.044 ± 0.23	**0.46 ± 0.44**
2015	343	1.6	0.27	**0.51 ± 0.31**	**0.25 ± 0.13**	**0.76 ± 0.31**	−0.44 ± 0.19	**0.88 ± 0.26**	−0.71 ± 0.16	−0.27 ± 0.32
2016	357	1.2	0.23	*0.059 ± 0.25*	**0.26 ± 0.13**	**0.32 ± 0.25**	−0.40 ± 0.17	**0.28 ± 0.24**	0.036 ± 0.18	−0.083 ± 0.27
2017	362	1.0	0.56	−0.24 ± 0.22	*−0.055 ± 0.16*	−0.30 ± 0.25	−0.50 ± 0.28	**0.33 ± 0.26**	0.16 ± 0.24	−0.013 ± 0.30
Years with negative or likely negative ΔS (%)				53	33	47	53	21[d]	29[d]	36
Years with positive or likely positive ΔS (%)				27	53	53	27	57[d]	29[d]	29
Years with indeterminate ΔS (%)				20	14	0	20	22[d]	42[d]	35

Note. Years with positive or likely positive ΔS in bold type; years with indeterminate ΔS in italics; years with negative or likely negative ΔS in regular type.

CGC, Central Grand Canyon; ECGC, East-Central Grand Canyon; EGC, Eastern Grand Canyon; LCR, Little Colorado River; LMC, Lower Marble Canyon; UMC, Upper Marble Canyon; WCGC, West-Central Grand Canyon.

[a]For sand budgeting, the downstream end of Grand Canyon is at the RK363 station and excludes the western part of Grand Canyon between the RK363 station and the Grand Wash Cliffs. [b]Incomplete sediment year; Colorado River continuous suspended-sediment monitoring began in August 2002. [c]These values calculated for the CGC segment. [d]These values calculated assuming equivalent ΔS between ECGC and WCGC during sediment years 2004–2007, when ΔS for only CGC could be calculated.

Table 3
Correlations (r) Between β_Q and Cumulative ΔS in Each Segment

Segment	r using upstream β_Q	r using average β_Q	r using downstream β_Q
UMC	[a]	[a]	−0.42 ($n = 322{,}449$)
LMC	−0.20 ($n = 322{,}450$)	−0.20 ($n = 275{,}980$)	−0.30 ($n = 314{,}549$)
EGC	[a]	[a]	0.13 ($n = 415{,}006$)
ECGC	−0.087 ($n = 353{,}556$)	−0.074 ($n = 312{,}272$)	0.097 ($n = 320{,}084$)
WCGC	−0.13 ($n = 320{,}084$)	−0.28 ($n = 296{,}920$)	−0.21 ($n = 308{,}428$)

Note. n indicates the number of observations.

All correlations are significant at the $p = 0.05$ critical level.

ECGC, East-Central Grand Canyon; EGC, Eastern Grand Canyon; LCR, Little Colorado River; LMC, Lower Marble Canyon; UMC, Upper Marble Canyon; WCGC, West-Central Grand Canyon.

[a]Upstream 15-min β_Q, and therefore also average 15-min β_Q, could not be calculated for UMC and EGC because the bed-sand grain size at the upstream ends of these segments is largely determined by the Paria River and LCR, respectively.

changes in upstream β_Q associated with fining in the leading edge or winnowing in the trailing edge of a sand wave should immediately reflect changes in sand mass in the downstream segment. Because it takes time for sand waves to transit a segment, however, there should be a lag between downstream β_Q and the total amount of sand stored in the upstream segment. Therefore, it is physically reasonable that the negative correlations between cumulative ΔS and upstream β_Q should be more universal than between cumulative ΔS and downstream β_Q.

Though the correlations between cumulative ΔS and β_Q make sense physically, these correlations are, at best, weak. This weakness is not unexpected given: (1) the larger absolute magnitude of the uncertainty in ΔS over longer timescales (Figure 8), and (2) the shorter lengths of the reaches over which β_Q applies relative to the longer lengths of the segments over which ΔS applies. The segments are 42–127 km long whereas the bed-sand grain size measured by β_Q applies to only the ∼1-km-long reach scale, that is, less than a few percent of the segment length. Furthermore, the bed-sand fining associated with the addition of sand to a segment increases the downstream export of sand from that segment owing to the strong nonlinear relation between bed-sand grain size and C_{SAND}. Thus, Q places a limit on the bed-sand fining and sand storage in a segment. At low Q, and therefore low Q_{SAND}, the bed sand could conceivably fine to approach the grain size of the tributary sand supply as sand storage continues to increase. However, at high Q, the amount of bed-sand fining, and thus the amount of sand storage, is limited by the increased sand export and more rapid depletion of the tributary-supplied finer sand (i.e., more rapid sand-wave migration). Finally, there are other episodic processes that act to weaken the expected negative correlation between cumulative ΔS and β_Q, namely, winnowing of the bed sand and the deposition of inversely graded flood deposits (Rubin et al., 1998; Topping et al., 1999; Topping, Rubin, Nelson et al., 2000; Topping, Rubin, & Vierra, 2000).

4.8. Relations Between Flow, Spatial Change in Bed-Sand Grain Size, and Change in Sand Mass

Sand continuity dictates that erosion and deposition are respectively caused by divergence and convergence in q_{SAND} (after Exner, 1920, 1925; Smith, 1970):

$$\frac{\partial \eta}{\partial t} = -\frac{1}{1 - \lambda_P}\left(\frac{\partial V_{SAND}}{\partial t} + \nabla \cdot q_{SAND}\right) \qquad (6)$$

where η is bed elevation, t is time, λ_P is bed-sand porosity, V_{SAND} is the one-dimensional total volume of sand in suspension over a point on the bed, and q_{SAND} is the depth-integrated local suspended-sand flux over the same point on the bed. Exner's (1920, 1925) version of Equation 6 was not completely correct because, in place of q_{SAND}, he used the depth-averaged velocity of water multiplied by a constant of proportionality (Paola & Voller, 2005; Smith, 1970); Exner (1925) stated that he used this constant for "simplification." Smith's (1970) derivation (his equation 1) is the earliest form of Equation 6 we found that includes all of

the terms required to conserve sediment mass among suspension, the bedload, and the bed, and is the form commonly referred to today as the Exner equation (Coleman & Nikora, 2009; Paola & Voller, 2005; Parker, 1991; Parker et al., 2000). $\partial V_{SAND} / \partial t$ in Equation 6 is neglected for our purposes because it is negligible compared to $\nabla \cdot q_{SAND}$ (following Rubin & Hunter, 1982). Though spatial changes in q_{SAND} are caused by spatial changes in τ_b under nonuniform flow conditions, they are instead associated with spatial changes in bed-sand grain size under uniform flow conditions and constant bed-sand area. We, therefore, evaluated whether the longitudinal gradients in bed-sand grain size produced by migrating sand waves were related to ΔS in the manner predicted by theory. For this analysis, we calculated the monthly mean Q at the downstream station and the monthly mean β_Q for the two stations bracketing a segment. We then segregated the data into 100 m³/s Q-bins; months with controlled floods were placed in their own bin because most sand transport in these months occurs during the controlled flood and is not related to monthly mean Q. So that the monthly mean β_Q values were representative of the monthly bed-sand conditions, this analysis was conducted only for those months where acoustical measurements at each station existed at ≥2,000 (i.e., ≥70%) of the 15-min intervals in that month.

Scaling of the one-dimensional form of Equation 6 under conditions of longitudinally constant u_*, flow depth, and bed-sand area (after Grams et al., 2013, and Equation 1 in Text S4) yields the proportionality:

$$\frac{\Delta \eta}{\Delta t} \propto -\frac{\Delta D_B^{-2.8}}{\Delta x} \tag{7}$$

where Δ indicates the change in a quantity and x is longitudinal position. The assumption of longitudinally constant u_*, flow depth, and bed-sand area is justified on the basis of similar monthly flow conditions among the stations and the reasoning in Section 1.2. ΔS is the change in sand mass over a given time interval Δt, and ΔS is the product of $\Delta \eta$ and the following constants: river width, segment length (Δx), sediment density, one minus the bed-sand porosity, and fractional bed-sand area. Thus, because β, like D_B, is a linear measure of the coarseness of the bed-sand grain-size distribution, making the appropriate substitutions and rearrangement of Equation 7 for the purposes of this analysis yields:

$$\text{monthly } \Delta S \propto -\Delta \beta_Q^{-2.8} \tag{8}$$

Because this analysis requires monthly mean β_Q at both ends of a segment and because the upstream β_Q in the UMC and EGC segments is respectively determined largely by the Paria River and LCR, and not determined by the bed sand at the RK0 and RK99 stations, we estimated β_Q at the upstream ends of these segments based on the sand loads of these tributaries. Monthly ΔS was positive for UMC whenever the Paria River supplied ≥100,000 Mg of sand, irrespective of Q or β_Q at the RK49 station. Likewise, monthly ΔS was positive for EGC whenever the LCR supplied ≥90,000 Mg of sand, irrespective of Q or β_Q at the RK141 station. Thus, we excluded months exceeding these thresholds from the UMC and EGC analyses because such large sand supplies likely caused extremely low values of upstream β_Q that we could not accurately estimate. For the other months of relative tributary quiescence, we estimated the upstream mean β_Q for UMC as ~2.5 (because the upstream bed sand was likely much coarser than at RK49), and we estimated the upstream mean β_Q for EGC as the value at the RK99 station (thus neglecting the influence of the LCR).

As predicted by Equation 8, downstream coarsening in a segment typically results in positive ΔS, whereas downstream fining typically results in negative ΔS (Figure 9). This result is indicated by the generally positive and significant slopes of the $-\Delta \beta_Q^{-2.8}$—ΔS relations and the fact that the data plot mostly in the lower-left and upper-right quadrants in Figure 9. Furthermore, smaller longitudinal gradients in bed-sand grain size at high Q are associated with the same ΔS as are larger longitudinal gradients in bed-sand grain size at low Q, as indicated by the Q-dependent increases in the slopes of the $-\Delta \beta_Q^{-2.8}$—ΔS relations. This positive relation between Q and the grain-size gradient required for similar ΔS is also behavior predicted by theory. Because Q_{SAND} is generally larger at higher Q, smaller longitudinal gradients in bed-sand grain size cause a similar unsigned magnitude of flux divergence, and therefore a similar magnitude of erosion or deposition, at high Q as would larger longitudinal gradients in bed-sand grain size at low Q.
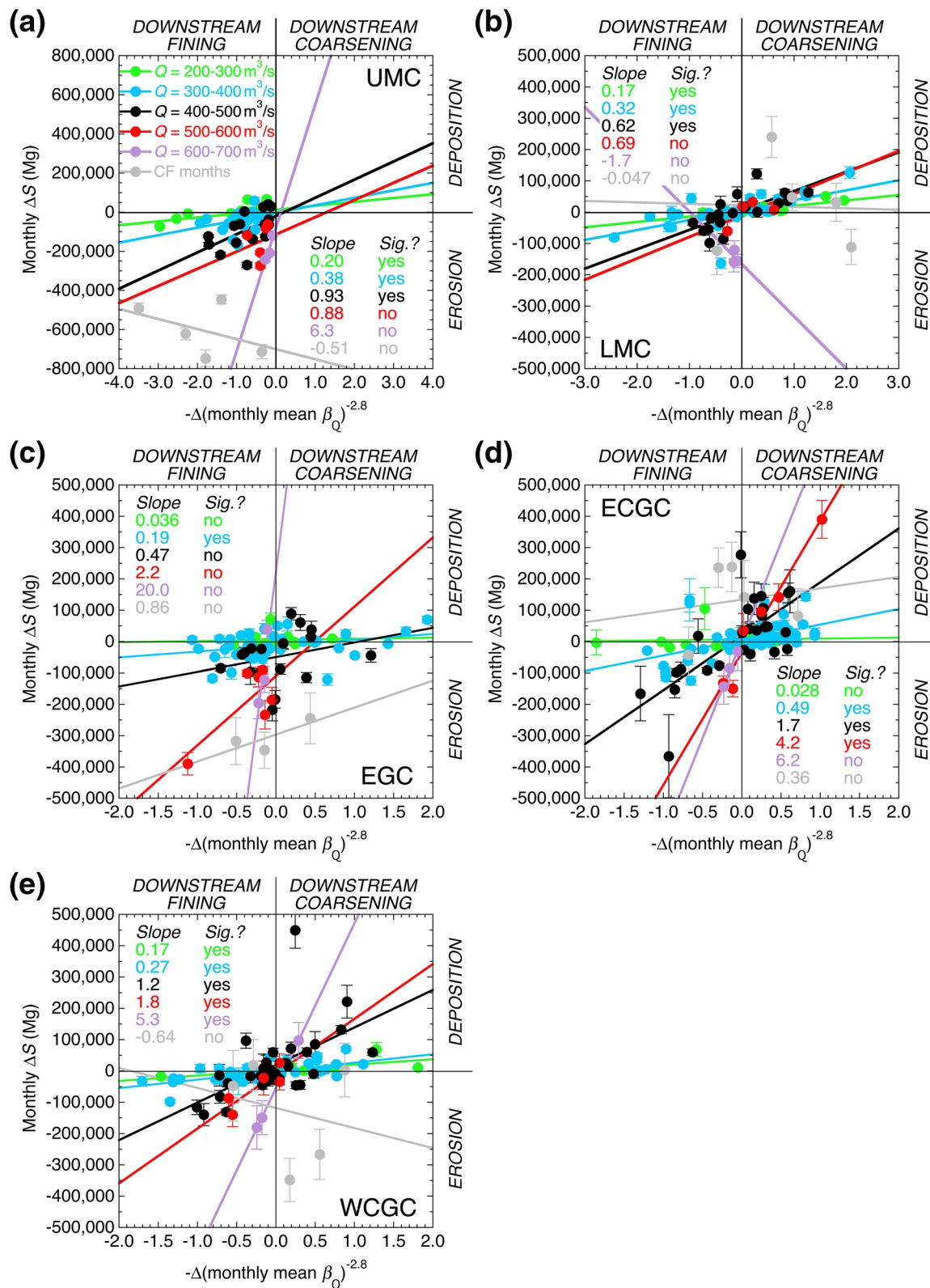
Figure 9. Q-binned monthly ΔS plotted as a function of $-\Delta$(monthly mean β_Q)$^{-2.8}$ in the (a) UMC, (b) LMC, (c) EGC, (d) ECGC, and (e) WCGC segments. Greater positive $-\Delta\beta_Q^{-2.8}$ corresponds to greater downstream coarsening, whereas greater negative $-\Delta\beta_Q^{-2.8}$ corresponds to greater downstream fining. Error bars indicate the uncertainty in ΔS propagated through Equation 5. Color-coded slopes and significance (at the $p = 0.05$ critical level) of the $-\Delta\beta_Q^{-2.8}$—ΔS relations in each Q bin are indicated. Listed slopes are divided by 100,000 for graphical simplicity. CF, controlled flood; ECGC, East-Central Grand Canyon; EGC, Eastern Grand Canyon; LMC, Lower Marble Canyon; UMC, Upper Marble Canyon; WCGC, West-Central Grand Canyon.
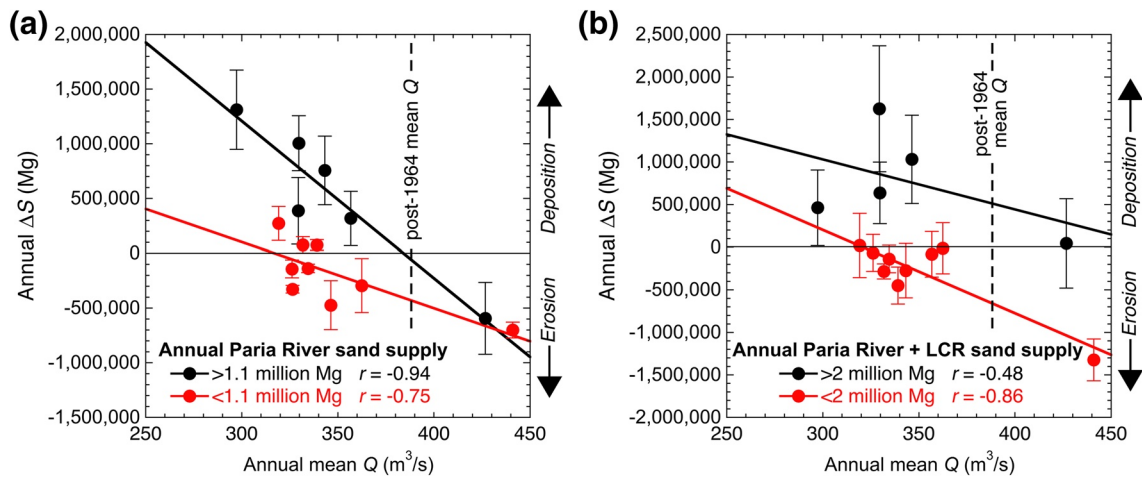
Figure 10. Annual ΔS plotted as a function of annual mean Q for the (a) Marble Canyon and (b) Grand Canyon segments. Data are segregated into high and low annual sand-supply categories, with least-squares linear regressions fit to each category and the correlation coefficient associated with each regression shown. Error bars indicate the magnitudes of the uncertainties in annual ΔS propagated through Equation 5.

4.9. Relations Between Flow, Tributary Sand Supply, and the Change in Sand Mass Over Longer Segments and Timescales

Bed-sand grain size weakly reflects the magnitude of sand storage (Table 3). Moreover, longitudinal gradients in bed-sand grain size associated with sand-wave migration largely control whether sand erodes or deposits (Figure 9). However, only minimal change in bed-sand grain size persists over multiple years despite the downstream migration of sand waves causing large shorter-term variation in bed-sand grain size important for sand transport, erosion, and deposition (Figure 7). This result, in combination with the systematic changes in grain size associated with sand-wave migration being smaller over longer longitudinal scales (Figure 5) allows relations to be developed between annual mean Q, tributary sand supply, and ΔS for all of Marble Canyon and Grand Canyon, neglecting the influence of bed-sand grain size. Despite the fact that predictions using these relations have larger error because they neglect grain-size effects and simplify the distribution of Q over each year to only one value, these relations are advantageous because they allow estimation of ΔS for periods lacking suspended- or bed-sand data (i.e., most of the period since the 1963 closure of Glen Canyon Dam).

ΔS is negatively correlated with mean Q over annual timescales, with the magnitude of the annual tributary sand supply segregating the data into two groups (Figure 10). On the basis of maximizing the |r| values among the Q—ΔS relations to best segregate the data into two groups, the threshold Paria River annual sand supply for Marble Canyon is 1.1 million Mg, and the threshold combined Paria River and LCR annual sand supply for Grand Canyon is 2 million Mg. Negative correlations between annual mean Q and annual ΔS in these two groups are very strong in Marble Canyon and moderate to very strong in Grand Canyon. Sand only accumulates in Marble Canyon during years when mean Q is less than ~380 m³/s and the Paria River supplies >1.1 million Mg of sand. At higher mean Q, sand erodes from Marble Canyon regardless of the magnitude of the annual sand supply. Similarly, sand only accumulates in Grand Canyon during years when mean Q is less than ~400 m³/s and the Paria River and LCR collectively supply >2 million Mg of sand. Importantly, these annual sand-supply thresholds are 124% of the Paria River mean-annual sand load and 136% of the combined Paria River and LCR mean-annual sand load, and the Q thresholds are near the post-1964 average of 388 m³/s released from Glen Canyon Dam. In lower sand-supply years, ΔS is typically indeterminate or negative at lower Q, and ΔS is negative at Q exceeding ~370 m³/s. Thus, well-above-average tributary sand-supply years and near-average or lower Q releases from the dam are likely required to maintain positive sand mass balances in Marble and Grand canyons. At lower-than-average Q, tributary sand inputs exceeding ~130% of average are apparently large enough to compensate for the increased sand export caused by the bed-sand fining resulting from these inputs. Furthermore, below-average Q

releases from the dam are likely required to prevent net erosion of sand from Marble and Grand canyons during years of below-average tributary sand supply.

Extension of this result to all years after dam construction suggests that net erosion of sand from Marble Canyon has occurred in ~69% of all years and net erosion of sand from Grand Canyon has occurred in ~52% of all years since the 1963 closure of Glen Canyon Dam. The strong to near-perfect correlations between annual mean Q and sand load for the Paria River and LCR were used estimate the sand supplies from these tributaries in these calculations (Text S13). The total estimated post-dam sand erosion is ~15 million Mg from Marble Canyon and ~13 million Mg from Grand Canyon, with most of this erosion occurring during the high-Q years of the 1980s and late 1990s (Text S13). Though this crude estimation approach predicts erosion consistent with that measured in Marble Canyon during the high-Q sediment year 1984 (Text S13), it does not predict the measured ~13 million Mg of sand eroded from Marble Canyon and EGC during the first higher-Q dam releases in 1965 (Grams et al., 2007; Topping et al., 2003) and underpredicts the amount of sand eroded from Grand Canyon during sediment year 1984. These gross underpredictions of erosion arise from this estimation approach neglecting the effects of the large changes in bed-sand grain size and possibly large reductions in bed-sand area that accompanied these periods of substantial erosion (Text S13). Thus, the estimated total ~28 million Mg of erosion is only a highly approximate lower bound for the actual net amount of sand eroded from Marble and Grand canyons during sediment years 1964–2017.

5. Discussion

5.1. Tributary-Generated Sand Waves

Our results confirm that, as originally suggested by Topping, Rubin, Nelson et al. (2000), sediment supplied during tributary floods travels rapidly downstream in the Colorado River as an elongating sediment wave, with components in the bed and in transport. Within this sediment wave, the silt-and-clay wave has a celerity slightly slower than the water velocity, with the front of the sand wave only slightly lagging the front of the silt-and-clay wave. Although the fine front of the sand wave migrates to Lake Mead within a week of a tributary flood (at ~3–3.5 km/hr), the coarser lagging part of the sand wave can be detected for hundreds of days in Marble and Grand canyons. The downstream migration of a sand wave is associated with large changes in grain size that regulate sand transport and storage in the bedrock-canyon Colorado River.

These results are largely consistent with previous empirical observations, observations in flumes, and with theory; the few discrepancies with theory arise because existing sediment-wave theory was developed for relatively high-Rouse number conditions. Existing sediment-wave theory does not predict the splitting of sand waves into two packets because it does not adequately incorporate the Rouse-number control on transport mode for grain-size distributions spanning the continuum from washload to bedload (Einstein & Chien, 1953a; Einstein et al., 1940; Woo et al., 1986). The mathematics that characterize the physics of such a broad-Rouse number model of sand-wave behavior were described by Topping et al. (2018). Under the Q range released from Glen Canyon Dam, the grain-size distribution of the tributary sand supply includes size classes transported as washload, resuspended bed sediment, and bedload in the Colorado River. Nevertheless, though existing sediment-wave theory does not predict the observed grain-size-controlled splitting of Colorado River sand waves, it does adequately describe the dispersion and translation observed in the coarser size classes that comprise packet B. As observed in flume run 4b of Cui, Parker, Lisle et al. (2003), a limited supply of higher-Rouse number sand transported over a coarser bed under lower-Froude number conditions forms a wave that broadens (i.e., exhibits dispersion) as it migrates (i.e., translates) downstream. We observed this behavior through the lagged-covariance analyses that detected the translation and dispersion of packet B's secondary covariance peak, behavior explained by the modified theory in Section 6 of Cui, Parker, Pizzuto et al. (2003) and consistent with Lisle (2007).

Though the splitting of sand waves into two packets is not predicted by existing sediment-wave theory, it is consistent with the Rouse-based suspended-sediment theory of McLean (1992). This theory illustrates that relatively little sand in the finest size classes is required on the bed to support a relatively large amount of these size classes in suspension. Because the typical D_S associated with packet A is ~0.09 mm, the Rouse numbers of the finest half of packet A in suspension thus range from 0.1 to 0.3 under common dam-released Q (Text S14). Under such Rouse numbers, there is relatively little concentration gradient in the vertical dimension, and these

size classes are transported as quasi-washload, transitional between washload and suspended bed sediment (e.g., Figures 3.18 and 4.10 in Topping, 1997). Thus, the bulk of the size classes comprising packet A are transported in suspension, with relatively little interaction with the bed sand. As observed in September 1999, the finer 50% of the suspended sand comprised only ∼0.85% of the bed sand at the front of packet A and comprised only ∼12% of the bed sand at the peak of packet A (Text S2). The most likely physical explanation for this behavior that likely controls the splitting of the sand waves into two packets is that the thickness of the active layer (Bennett & Nordin, 1977) varies in a quasi-step-change fashion as a function of grain size. The finest size classes of sand with the lowest, near-washload Rouse numbers have excursion lengths that likely exceed the wavelengths of the dunes (Mohrig & Smith, 1996; Naqshband, Hoitink et al., 2017; Naqshband, McElroy et al., 2017), thereby bypassing the dunes and limiting the depth to which these size classes mix into the bed during sand-wave migration. Consequently, the thickness of the active layer will roughly equal the maximum dune height (Church & Haschenburger, 2017) for the coarser size classes that comprise packet B but will be negligible for the finest sand size classes that comprise packet A, a hypothesis to be tested in future numerical model development using the equations in Topping et al. (2018).

5.2. Implications of Sand-Wave Migration for the Timing of Controlled Floods Conducted to Rebuild Sandbars

The finest bed sand is associated with the largest C_{SAND} and highest sandbar-deposition rates during controlled floods (after Grams et al., 2015, 2013; Schmidt et al., 1993; Topping, Rubin, Nelson et al., 2000; Topping, Rubin, & Vierra, 2000; Topping et al., 2019, 2007). During our study, maximum bed-sand fining in packet B occurred at the RK49 and RK99 stations ∼63 and 144 days, respectively, after a large Paria River flood (Figure 5b). Thus, controlled floods conducted <63 days after a large Paria River flood will likely result in the largest sandbars upstream from the RK49 station in UMC, whereas controlled floods conducted between 63 and 144 days after a large Paria River flood will likely result in the largest sandbars between the RK49 and RK99 stations in LMC. However, because C_{SAND} depends primarily on Q and secondarily on bed-sand grain size (Section 4.2), the temporal window for conducting controlled floods for maximum sandbar deposition could be lengthened if dam-released Q were decreased between the Paria River flood(s) and the controlled flood (Rubin et al., 2002).

5.3. Implications of Sand-Wave Migration for Grain-Size Patterns During Floods, and for the Grain-Size Architecture of Bedrock-Canyon Alluvium

Peak Q lags the sand supply during both natural and dam-released floods (Topping, Rubin, & Vierra, 2000; Topping et al., 2010, 2005). The ramification of this lag is that peak Q occurs long after the downstream export of packet A from our study area and typically during the migration of the trailing edge of packet B, where the bed sand coarsens in the upstream direction. As the result of this downstream fining, C_{SAND} increased in the downstream direction during the rising limb of pre-dam snowmelt floods (Topping, Rubin, & Vierra, 2000), and C_{SAND} also typically increases in the downstream direction during controlled floods depending on the longitudinal location of the peak of packet B (Topping et al., 2010). The acute supply limitation of the finer sand size classes caused by the downstream-fining-driven increase in C_{SAND} feeds back to cause winnowing of the bed sand. Greater winnowing of the finest size classes from the bed thus occurs as packet B migrates more quickly during floods (Rubin et al., 1998; Topping, Rubin, Nelson et al., 2000). This enhanced bed coarsening causes C_{SAND} to decrease and the suspended sand to coarsen over time, thereby producing inversely graded deposits both during natural pre-dam and dam-released floods (Draut & Rubin, 2013; Rubin et. al., 1998; Topping, Rubin, Nelson et al., 2000; Topping et al., 2010, 1999; Topping et al., 2005, 2006). These deposits laterally erode upon flood recession, re-exposing the finer underlying sand (Topping et al., 1999, 2005, 2007). Partial preservation of these deposits persists for decades (Topping, Rubin, Nelson et al., 2000; Topping et al., 2005), and in isolated circumstances for up to ∼4,500 years (O'Connor et al., 1994). Though seemingly long, this retention of minor amounts of sand in a bedrock-canyon river is still transient compared to the much longer sand retention possible in alluvial rivers (Bradley & Tucker, 2013).

The depth of bed-sand winnowing during sand-wave migration likely controls the vertical grain-size architecture of the alluvial cover in bedrock-canyon rivers, thus leading to large variance in bed-sand grain size for a given magnitude of sand storage. Although the overall grain-size architecture of Colorado River alluvium fines upward from the channel bed to the banks (Rubin et al., 2020, 1998), individual deposits on the bed, bars, and banks may coarsen upward. The thickness of the active layer (Bennett & Nordin, 1977) scales with dune height (Church & Haschenburger, 2017), and the dune height during Colorado River floods (Topping et al., 2007) is less than the maximum bed-sand thickness (Grams et al., 2013). Therefore, it is likely that winnowing during floods does not affect the full thickness of the sand everywhere. Depending on the scour depth during successive floods, the interaction of floods with migrating sand waves thus leads to a likely multilayer, inversely graded (i.e., armored) architecture. The presence of inversely graded deposits means that the volume and the surface grain size of the sand in storage may be positively correlated. Therefore, "more sand" may not always equate to the presence of finer sand on the surfaces of the bed, bars, and banks (Section 4.7; Topping et al., 2005, 2008), and long-term fining trends (Section 4.5) may not indicate sand-storage increases.

5.4. Regulation of Suspended-Sand Concentration Arising from Changes in Discharge and Bed-Sand Grain Size

Studies in a number of rivers in the western United States have shown that the bed-sand grain-size distribution can play an important role in regulating sand transport (Dean et al., 2016; Rubin and Topping, 2001, 2008; Topping, Rubin, Nelson et al., 2000; Topping et al., 2007, 2018). Herein, we document two different styles of change in bed-sand grain size that affect C_{SAND}, one arising simply from changes in Q and the other arising from the migration of tributary-generated sand waves.

Both direct measurements and β indicate that there is a general tendency for the bed sand in the Colorado River to fine as Q increases, and that this fining is manifest mainly by an increase in the finest size classes. Three possibilities exist to explain this behavior: (1) increasing Q erodes finer sand from sandbars and higher-elevation deposits (Andrews et al., 1999) that then mixes with the bed sand (Topping et al., 1999, 2010); (2) increasing Q disrupts the bed armoring that was produced from winnowing (Rubin et al., 1998) by increasing the thickness of the active layer over which the bed sand mixes (Bennett & Nordin, 1977) as dune height increases (Topping et al., 2007); or (3) increasing Q disrupts the bed armoring produced from winnowing by scouring the sand stored in deeper pools (Topping, Rubin, Nelson et al., 2000). The finer sand scoured by process (3) is then redistributed to other parts of the bed (Topping, Rubin, Nelson et al., 2000), thus causing the increase in bed-sand area at higher Q observed by Anima et al. (1998) and Schmidt et al. (2007). Regardless of its genesis, the bed-sand fining detected as a ~38% decrease in β over a factor of 8.5 increase in Q causes C_{SAND} to increase by a factor of ~3.8 (Equation 1 in Text S4).

Though the changes in bed-sand grain size caused by Q are important, the downstream migration of sand waves causes much larger changes in bed-sand grain size that are, in turn, associated with much larger changes in C_{SAND}. Direct bed-sediment measurements and β_Q both indicate a typical change in bed-sand grain size of a factor of ~3 (Figure 7, Text S11) in response to sand-wave migration. This magnitude of change in either D_B or β_Q is associated with a factor of ~22 change in C_{SAND} (Equation 1 in Text S4). Depending on exactly how the fine tail of the grain-size distribution changes, however, a change in D_B of only a factor of two can be associated with much larger changes in C_{SAND} (factor of ~30; Topping et al., 2007).

These two styles of grain-size change together lead to the $|\alpha|$ values ranging from 0.2 to 0.4 for the EDI/EWI/VPA and calibrated-pump measurements. Over the factor of ~8.5 range in Q in Figure 4, a factor of ~300 change in C_{SAND} (Equation 1 in Text S4) is caused by the factor of ~3.8 change in u_* associated with this change in Q (Text S3). Over this same range in Q, a combined factor of ~84 change in C_{SAND} is caused by the changes in bed-sand grain size arising from changes in Q and sand-wave migration. Simple division of the amount of change in C_{SAND} caused by bed-sand grain size (factor of ~84) by the amount of change in C_{SAND} caused by Q (factor of ~300) yields 0.28, a value consistent with the 0.2 to 0.4 range in $|\alpha|$.
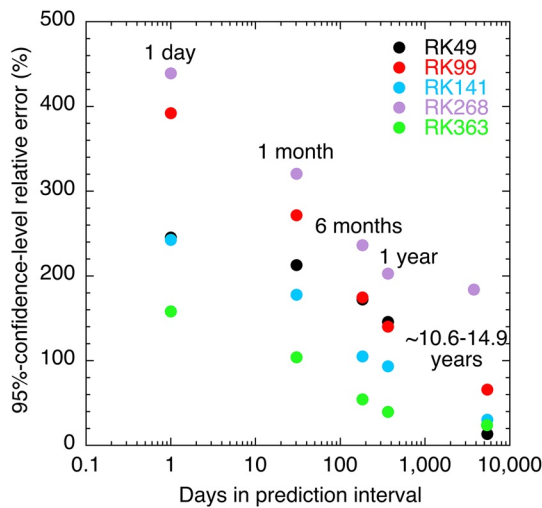
Figure 11. 95%-confidence-level relative error in the rating-curve estimations of suspended-sand load in each prediction interval. These values calculated from those in Figure 3 in Text S15 assuming a Gaussian normal error distribution. The prediction intervals of 1 day, 1 month, 6 months, 1 year, and the entire period of record (~10.6–14.9 years depending on the station) are indicated.

5.5. Self-Limiting Sand Storage Arising From Grain-Size Effects

The weak relation between bed-sand grain size and sand-storage magnitude combines with the much stronger control of longitudinal changes in bed-sand grain size on erosion/deposition to regulate sand storage. As a result, sand storage in the bedrock-canyon Colorado River is self-limiting at any given Q, with larger amounts of sand storage possible at lower Q. Tributary resupply of sand to the Colorado River increases the amount of sand in storage and decreases the bed-sand grain size. Thus, though finer bed sand is typically associated with more sand, finer bed sand also causes substantially higher sand transport. As a result of the higher sand transport at higher Q, smaller longitudinal gradients in bed-sand grain size are required to promote relatively larger changes in sand storage at higher Q. This key Exner-based result is why sand waves migrate faster at higher Q. The longitudinal gradients in bed-sand grain size in a tributary-generated sand wave (downstream coarsening in the leading edge of a packet followed by downstream fining in the trailing edge) result in deposition followed by erosion as a sand wave migrates downstream. Thus, sand waves migrate faster at higher Q because the amount of sand in a sand wave is finite and similar longitudinal gradients in bed-sand grain size will be associated with larger amounts of deposition or erosion at higher Q.

Sand storage in bedrock-canyon rivers like the Colorado River is therefore self-limiting. In essence, though adding finer sand increases the amount of sand storage, this addition of finer sand also increases the sand export, with export also increasing with Q. Thus, sand storage within a bedrock canyon is limited by Q and the episodic sand resupply. This self-limiting behavior also occurred before the construction of Glen Canyon Dam. Despite the fact that the Colorado River transported ~20–30 times its modern dam-altered sand supply, sand only accumulated in the pre-dam Colorado River at lower Q and was supply limited at higher Q (Topping, Rubin, & Vierra, 2000).

5.6. Need for Continuous Sand-Transport Data

Calculation of sand loads sufficiently accurate for the construction of meaningful mass-balance sand budgets requires continuous measurements of C_{SAND} owing to the systematic supply-driven changes in C_{SAND} discussed above. The importance of this requirement is inversely related to the duration of the prediction interval over which accurate sand loads and budgets are needed (Figure 11), as indicated by the comparison of the suspended-sand loads estimated by log-linear relations between Q and C_{SAND} (sand rating curves) with the loads calculated from continuous measurements (Text S15). The sand rating curves used in this analysis were derived using standard methods (Helsel & Hirsch, 2002), and were fit to the first 3 years of EDI/EWI measurements of C_{SAND} at each station. The 95%-confidence-level relative error in the rating-curve-estimated load decreased in a semi-log-linear fashion at each station as the prediction interval increased (Figure 11). Regardless of this inverse relation between error and prediction interval, the errors in the rating-curve-estimated suspended-sand loads over all prediction intervals in Figure 11 are so large that they prevent knowing the sign, let alone the magnitude of ΔS.

This finding agrees with that of Grams et al. (2019) who showed that C_{SAND} must be measured continuously over short timescales for the sand-transport "signal" to exceed "noise," but largely contradicts those of Cohn et al. (1992), Horowitz (2003), Cohn (1995), and Horowitz et al. (2015) who concluded that accurate loads could be calculated using rating curves that utilized relatively few measurements. In justifying the use of sediment rating curves, Cohn et al. (1992) stated that errors in measured loads can be large owing to the sampling error of individual observations, whereas rating-curve errors may be smaller because they are based on the entire dataset. That argument assumed random variability in C_{SAND} about rating curves, an incorrect assumption in rivers where C_{SAND} is regulated by a process other than Q. Hirsch (1988) showed that accurate constituent rating curves required both a large dataset and incorporation of systematic hysteresis effects. Wright et al. (2010) showed that reasonably accurate sand rating curves could be constructed for supply-limited

conditions given a large dataset that allowed for the inclusion of supply-driven hysteresis. Both of these data-intensive approaches produce, in essence, time-variant sediment rating curves. However, in many applications the dataset used to define rating curves is relatively sparse and/or hysteresis effects are not included; indeed, the attraction of the sediment–rating-curve approach is that it is inexpensive (Cohn, 1995) and curves can be developed with relatively little data. Given the intensive data requirements for the approaches of Hirsch (1988) or Wright et al. (2010), and because it is impossible to know whether this sampling requirement has been met without a large investment in many measurements of C_{SAND}, it is best to rely on continuous measurements of C_{SAND} when initiating river sediment monitoring.

6. Conclusions

Sand supplied during tributary floods migrates downstream in the Colorado River downstream from Glen Canyon Dam as a sand wave that splits into two packets on the basis of Rouse number. The leading packet migrates downstream at nearly the velocity of water, with some newly supplied sand in this packet never being retained in the Colorado River. The lagging packet migrates more slowly and takes hundreds of days to be exported to Lake Mead. Substantial changes in the bed-sand grain size distribution occur as these packets migrate, leading to in excess of an order-of-magnitude discharge-independent variation in suspended-sand concentration. Although the analyses we use herein can inform the design of sediment-transport monitoring programs, there is no "short cut" to monitoring sediment transport in a river with such large, systematic supply-driven variation in suspended-sand concentration; ongoing continuous suspended-sediment measurements are required. The bed-sand fining caused by sand-wave migration persists for <63 days in UMC and <144 days in LMC. Thus, only those controlled floods released from the dam within several months of a large Paria River flood will have access to the finest sand size classes that lead the highest suspended-sand concentrations, and hence the largest sandbar-deposition rates in Marble Canyon.

Sand storage in the bedrock-canyon Colorado River in Marble and Grand canyons is largely self-limiting. Fining of the bed-sand grain size as sand storage increases leads to higher suspended-sand concentrations, and therefore greater downstream sand export, a negative-feedback mechanism likely operating in other bedrock-canyon rivers. Except in the river segments proximal to the major sand-supplying tributaries, bed-sand grain size plays a dominant role in regulating whether sand erodes or deposits in the Colorado River. By virtue of this self-limitation, substantial increases in sand storage, as occurred during periods of low discharge pre-dam, are likely impossible in the Colorado River in Marble and Grand canyons at the higher discharges generally released from Glen Canyon Dam. Multiyear sand accumulation is only possible in the Colorado River in GCNP during years when the tributary sand supply exceeds ~130% of average and dam-released discharges are below average. Sand erodes during years of below-average to average tributary sand supply and average to above-average discharge; net erosion of at least 28 million Mg of sand from the Colorado River in GCNP has occurred since the 1963 closure of Glen Canyon Dam. Thus, sand storage sufficient for maintaining sandbars in the Colorado River may require timing periods of higher and lower dam-released discharge based on tributary sand-supply conditions. Whether the sand resources of the Colorado River in GCNP can be sustainably managed in perpetuity therefore remains an open question.

Notation

CGC	Central Grand Canyon segment
ECGC	East-Central Grand Canyon segment
EDI	Equal-Discharge-Increment suspended-sediment measurement
EGC	Eastern Grand Canyon segment
EWI	Equal-Width-Increment suspended-sediment measurement
GCNP	Grand Canyon National Park
LCR	Little Colorado River
LMC	Lower Marble Canyon segment
RK	river kilometer
UMC	Upper Marble Canyon segment

VPA	Velocity-weighted-average Point-sample Array suspended-sediment measurement
WCGC	West-Central Grand Canyon segment
A_i	variable A at position i in a time series (dimensions vary between lagged-covariance analyses in paper and Text S8)
$\bar{A}$	mean of variable A_i over the entire time series (dimensions vary between lagged-covariance analyses in paper and Text S8)
A_m	area of active deposits measured for topographic change in Text S12 (L^2)
A_T	total area of active deposits in Text S12 (L^2)
a_0	constant of proportionality in Text S4
a_1	constant of proportionality in Text S4
B_i	variable B at position i in a time series (dimensions vary between lagged-covariance analyses in paper and Text S8)
$\bar{B}$	mean of variable B_i over the entire time series (dimensions vary between lagged-covariance analyses in paper and Text S8)
C_{SAND}	velocity-weighted suspended-sand concentration (ML^{-3})
$C_{SAND-REF}$	reference, i.e., mean, C_{SAND} over a specified period (ML^{-3})
$C_{SILT-CLAY}$	velocity-weighted suspended-silt-and-clay concentration (ML^{-3})
D	grain diameter (L)
D_0	reference grain diameter of 1 mm in ϕ unit
D_B	median grain size of the bed sand (L)
D_{B-REF}	reference, i.e., mean, D_B over a specified period (L)
D_S	median grain size of the suspended sand (L)
D_{S-REF}	reference, i.e., mean, D_S over a specified period (L)
D_X	X^{th} percentile grain size (L)
E	downstream sand export from a river segment over a given period (M)
f	fractional amount, expressed as a percentage, of the bed sand composed of a given size class (dimensionless)
f_{VF}	fractional amount, expressed as a percentage, of the bed sand composed of very fine, i.e., 0.0625–0.125 mm, sand (dimensionless)
h	flow depth in Text S3 (L)
I	upstream sand supply to a river segment over a given period (M)
I_{LT}	sand supply from lesser tributaries to a river segment over a given period (M)
I_T	sand supply from major tributaries to a river segment over a given period (M)
i	number indicating position in a time series; used in lagged-covariance analysis
J	4.3; value used in Equation 1 and in Text S4
j	number indicating position in a time series relative to a given position i; used in lagged-covariance analysis
K	−2.8; value used in Equation 1 and in Text S4
k	0.408; von Karman's constant (dimensionless)
L	0.18; value used in Equation 1 and in Text S4
M	0.85; value used in Equation 1 and in Text S4
N	number of total 15-min intervals analyzed in lagged-covariance analysis
n	number of observations
p	level of significance
p_R	Rouse number in Text S14 (dimensionless)
Q	discharge of water (L^3t^{-1})
Q_{SAND}	cross-section-integrated mass flux of sand (Mt^{-1})
q_{SAND}	depth-integrated local flux of suspended sand over a point on the bed (L^2t^{-1})
$Q_{SILT-CLAY}$	cross-section-integrated mass flux of suspended silt and clay (Mt^{-1})
r	correlation coefficient
t	time (t)
u	downstream component of the flow velocity vector in Text S3 (Lt^{-1})
u_*	shear velocity (Lt^{-1})
V_{SAND}	1-dimensional total volume of suspended sand over a point on the bed (L)

w_s	sediment settling velocity in Text S14 (Lt^{-1})
x	longitudinal position in the downstream direction (L)
$\bar{\bar{z}}_m$	area-weighted mean change in elevation where topographic or bathymetric measurements were made in Text S12 (L)
z_0	bed roughness parameter in Text S3 (L)
α	measure of the relative importance of bed-sand grain size versus shear velocity in regulating sand transport (dimensionless)
β	measure of the relative coarseness of the bed sand (dimensionless)
β_Q	β detrended as a function of water discharge (dimensionless)
ΔS	change in the amount of sand, i.e., the sand mass balance, in a river segment over a given period (M)
ΔS_m	measured topographic-based sand budget in Text S12 (L^3)
ΔS_{mEx}	extrapolated topographic-based sand budget in Text S12 (L^3)
Δt	time interval in lagged-covariance analysis (t)
ϕ	phi unit of sediment grain size (Krumbein, 1934); $\phi = -\log_2\left(D / D_0\right)$
η	bed elevation (L)
λ_P	bed-sand porosity (dimensionless)
ρ	water density
σ	standard deviation
$\sigma_{\Delta ms}$	uncertainty in the extrapolated topographic-based sand budget in Text S12 (L^3)
τ_b	boundary shear stress ($ML^{-1}t^{-2}$)

Data Availability Statement

All data collected during the 1996–2017 period of our study and analyzed herein are available at https://www.gcmrc.gov/discharge_qw_sediment/.

References

Andrews, E. D., Johnston, C. E., Schmidt, J. C., & Gonzales, M. (1999). Topographic evolution of sand bars. In R. H. Webb, J. C. Schmidt, G. R. Marzolf, & R. A. Valdez (Eds.), *The Controlled Flood in Grand Canyon, Geophysical Monograph*, 110 (pp. 117–130). Washington, DC: American Geophysical Union. https://doi.org/10.1029/GM110p0117

Anima, R. J., Marlow, M. S., Rubin, D. M., & Hogg, D. J. (1998). Comparison of sand distribution between April 1994 and June 1996 along six reaches of the Colorado River in Grand Canyon, Arizona. *U.S. Geological Survey Open-File Report 98-141* (33 pp.). https://doi.org/10.3133/ofr98141

Ashley, T. C., McElroy, B., Buscombe, D., Grams, P. E., & Kaplinski, M. (2020). Estimating bedload from suspended load and water discharge in sand bed rivers. *Water Resources Research*, 56, e2019WR025883. https://doi.org/10.1029/2019WR025883

Barnhardt, W. A., Kayen, R., Rubin, D., & Minasian, D. L. (2001). The internal structure of sand bars on the Colorado River, Grand Canyon, as determined by ground-penetrating radar. *U.S. Geological Survey Open-File Report 2001-425* (74 pp.). https://doi.org/10.3133/ofr01425

Bennett, J. P., & Nordin, C. F. (1977). Simulation of sediment transport and armouring. *Hydrological Sciences Bulletin*, 22, 555–569. https://doi.org/10.1080/02626667709491760

Beverage, J. P., & Culbertson, J. K. (1964). Hyperconcentrations of suspended sediment. *Journal of the Hydraulics Division, Proceedings of the American Society of Civil Engineers*, 90, 117–128.

Bradley, D. N., & Tucker, G. E. (2013). The storage time, age, and erosion hazard of laterally accreted sediment on the floodplain of a simulated meandering river. *Journal of Geophysical Research: Earth Surface*, 118, 1308–1319. https://doi.org/10.1002/jgrf.20083

Carothers, S. W., & Brown, B. T. (1991). *The Colorado River through Grand Canyon: Natural history and human change*. Tucson, AZ: University of Arizona Press.

Church, M., & Haschenburger, J. K. (2017). What is the "active layer"? *Water Resources Research*, 53, 5–10. https://doi.org/10.1002/2016WR019675

Cohn, T. A. (1995). Recent advances in statistical methods for the estimation of sediment and nutrient transport in rivers. *Reviews of Geophysics*, 33, 1117–1123. https://doi.org/10.1029/95RG00292

Cohn, T. A., Caulder, D. L., Gilroy, E. J., Zynjuk, L. D., & Summers, R. M. (1992). The validity of a simple statistical model for estimating fluvial constituent loads: An empirical study involving nutrient loads entering Chesapeake Bay. *Water Resources Research*, 28, 2353–2363. https://doi.org/10.1029/92WR01008

Coleman, S. E., & Nikora, V. I. (2009). Exner equation: A continuum approximation of a discrete granular system. *Water Resources Research*, 45, W09421. https://doi.org/10.1029/2008WR007604

Cross, W. F., Baxter, C. V., Rosi-Marshall, E. J., Hall, R. O., Jr., Kennedy, T. A., Donner, K. C., et al. (2013). Food-web dynamics in a large river discontinuum. *Ecological Monographs*, 83, 311–337. https://doi.org/10.1890/12-1727.1

Cui, Y., Parker, G., Lisle, T. E., Gott, J., Hansler-Ball, M. E., & Pizzuto, J. E. (2003). Sediment pulses in mountain rivers: 1. Experiments. *Water Resources Research*, 39, 1239. https://doi.org/10.1029/2002WR001803

Cui, Y., Parker, G., Pizzuto, J., & Lisle, T. E. (2003). Sediment pulses in mountain rivers: 2. Comparison between experiments and numerical predictions. *Water Resources Research*, 39, 1240. https://doi.org/10.1029/2002WR001805

Curry, C. W., Bennett, R. H., Hulbert, M. H., Curry, K. J., & Faas, R. W. (2004). Comparative study of sand porosity and a technique for determining porosity of undisturbed marine sediment. *Marine Georesources and Geotechnology*, *22*, 231–252. https://doi.org/10.1080/10641190490900844

Dean, D. J., & Topping, D. J. (2019). Geomorphic change and biogeomorphic feedbacks in a dryland river: The Little Colorado River, Arizona, USA. *Geological Society of America Bulletin*, *131*, 1920–1942. https://doi.org/10.1130/B35047.1

Dean, D. J., Topping, D. J., Schmidt, J. C., Griffiths, R. E., & Sabol, T. A. (2016). Sediment supply versus local hydraulic controls on sediment transport and storage in a river with large sediment loads. *Journal of Geophysical Research: Earth Surface*, *121*, 82–110. https://doi.org/10.1002/2015JF003436

Dietrich, W. E. (1982). Settling velocity of natural particles. *Water Resources Research*, *18*, 1615–1626. https://doi.org/10.1029/WR018i006p01615

Dietrich, W. E., Bellugi, D. G., Sklar, L. S., Stock, J. D., Heimsath, A. M., & Roering, J. J. (2003). Geomorphic transport laws for predicting landscape form and dynamics. In P. R. Wilcock & R. M. Iverson (Eds.), *Prediction in geomorphology, Geophysical Monograph*, 135 (pp. 103–129). Washington, DC: American Geophysical Union. https://doi.org/10.1029/135GM09

Dolan, R., Howard, A., & Gallenson, A. (1974). Man's impact on the Colorado River in the Grand Canyon. *American Scientist*, *62*, 392–401. https://www.jstor.org/stable/27844987

Dolan, R., Howard, A. D., & Trimble, D. (1978). Structural control of the rapids and pools of the Colorado River in the Grand Canyon. *Science*, *202*, 629–631. https://doi.org/10.1126/science.202.4368.629

Draut, A. E., & Rubin, D. M. (2013). Assessing grain-size correspondence between flow and deposits of controlled floods in the Colorado River, USA. *Journal of Sedimentary Research*, *83*, 962–973. https://dx.doi.org/10.2110/jsr.2013.79

Duan, N. (1983). Smearing estimate: A nonparametric retransformation method. *Journal of the American Statistical Association*, *78*, 605–1610. https://doi.org/10.1080/01621459.1983.10478017

East, A. E., Collins, B. D., Sankey, J. B., Corbett, S. C., Fairley, H. C., & Caster, J. C. (2016). Conditions and processes affecting sand resources at archeological sites in the Colorado River corridor below Glen Canyon Dam, Arizona. *U.S. Geological Survey Professional Paper 1825* (104 pp.). https://doi.org/10.3133/pp1825

Edwards, T. K., & Glysson, G. D. (1999). Field methods for measurement of fluvial sediment. *Techniques of Water-Resources Investigations of the U.S. Geological Survey 03-C2* (89 pp.). https://doi.org/10.3133/twri03C2

Einstein, H. A., Anderson, A. G., & Johnson, J. W. (1940). A distinction between bed-load and suspended load in natural streams. *EOS, Transactions of the American Geophysical Union*, *21*, 628–633. https://doi.org/10.1029/TR021i002p00628

Einstein, H. A., & Chien, N. (1953a). Can the rate of wash load be predicted from the bed-load function? *EOS, Transactions of the American Geophysical Union*, *34*, 876–882. https://doi.org/10.1029/TR034i006p00876

Einstein, H. A., & Chien, N. (1953b). Transport of sediment mixtures with large ranges of grain size. *Missouri River District Sediment Series* (Vol. 2, 72 pp.). Berkeley, CA: University of California.

Emery, W. J., & Thomson, R. E. (2001). *Data analysis methods in physical oceanography*. 2nd ed. Elsevier Science.

Exner, F. M. (1920). Zur physik der dünen. *Akademie der Wissenschaften in Wien, Mathematisch-Naturwissenschaftliche Klasse Sitzungsberichte Abt. IIa*, *129*, 929–952.

Exner, F. M (1925). Uber die wechselwirkung zwischen wasser und geschiebe in flüssen. *Akademie der Wissenschaften in Wien, Mathematisch-Naturwissenschaftliche Klasse Sitzungsberichte Abt. IIa*, *134*, 165–203.

Garrett, W. B., Van De Vanter, E. K., & Graf, J. B. (1993). Streamflow and sediment-transport data, Colorado River and three tributaries in Grand Canyon, Arizona, 1983 and 1985–86. *U.S. Geological Survey Open-File Report 93-174* (624 pp.). https://doi.org/10.3133/ofr93174

Graf, J. B. (1995). Measured and predicted velocity and longitudinal dispersion at steady and unsteady flow, Colorado River, Glen Canyon Dam to Lake Mead. *Water Resources Bulletin*, *31*, 265–281. https://doi.org/10.1111/j.1752-1688.1995.tb03379.x

Grams, P. E., Buscombe, D., Topping, D. J., Kaplinski, M., & Hazel, J. E., Jr. (2019). How many measurements are required to construct an accurate sand budget in a large river? Insights from analyses of signal and noise. *Earth Surface Processes and Landforms*, *44*, 160–178. https://doi.org/10.1002/esp.4489

Grams, P. E., Schmidt, J. C., & Topping, D. J. (2007). The rate and pattern of bed incision and bank adjustment on the Colorado River in Glen Canyon downstream from Glen Canyon Dam. *Geological Society of America Bulletin*, *119*, 556–575. https://doi.org/10.1130/B25969.1

Grams, P. E., Schmidt, J. C., Wright, S. A., Topping, D. J., Melis, T. S., & Rubin, D. M. (2015). Building sandbars in the Grand Canyon. *EOS, Transactions of the American Geophysical Union*, *96*, 12–16. Retrieved from https://eos.org/wp-content/uploads/2015/06/2015EO11.pdf?adaf16

Grams, P. E., Topping, D. J., Schmidt, J. C., Hazel, J. E., Jr., & Kaplinski, M. (2013). Linking morphodynamic response with sediment mass balance on the Colorado River in Marble Canyon: Issues of scale, geomorphic setting, and sampling design. *Journal of Geophysical Research: Earth Surface*, *118*, 361–381. https://doi.org/10.1002/jgrf.20050

Grams, P. E., & Wilcock, P. R. (2007). Equilibrium entrainment of fine sediment over a coarse immobile bed. *Water Resources Research*, *43*, W10420. https://doi.org/10.1029/2006WR005129

Grams, P. E., & Wilcock, P. R. (2014). Transport of fine sediment over a coarse, immobile river bed. *Journal of Geophysical Research: Earth Surface*, *119*, 188–211. https://doi.org/10.1002/2013JF002925

Grand Canyon Protection Act. (1992). Public Law No. 102-575, 106 Stat 4669–4673. Retrieved from https://www.govinfo.gov/content/pkg/STATUTE-106/pdf/STATUTE-106-Pg4600.pdf

Griffiths, R. E., & Topping, D. J. (2015). Inaccuracies in sediment budgets arising from estimations of tributary sediment inputs: An example from a monitoring network on the southern Colorado Plateau. *Proceedings of the 3rd Joint Federal Interagency Conference on Sedimentation and Hydrologic Modeling, April 19–23* (pp. 583–594). Reno, NV: Peppermill Hotel. Retrieved from https://acwi.gov/sos/pubs/3rdJFIC/Contents/4A-Griffiths.pdf

Griffiths, R. E., & Topping, D. J. (2017). Importance of measuring discharge and sediment transport in lesser tributaries when closing sediment budgets. *Geomorphology*, *296*, 59–73. https://doi.org/10.1016/j.geomorph.2017.08.037

Griffiths, R. E., Topping, D. J., Anderson, R. S., Hancock, G. S., & Melis, T. S. (2014). Design of a sediment-monitoring gaging network on ephemeral tributaries of the Colorado River in Glen, Marble, and Grand Canyons, Arizona. *U.S. Geological Survey Open-File Report 2014-1137* (21 pp.). http://dx.doi.org/10.3133/ofr20141137

Griffiths, R. E., Topping, D. J., Andrews, T., Bennett, G. E., Sabol, T. A., & Melis, T. S. (2012). Design and maintenance of a network for collecting high-resolution suspended-sediment data at remote locations on rivers, with examples from the Colorado River. *U.S. Geological Survey Techniques and Methods 8-C2* (44 pp.). https://doi.org/10.3133/tm8c2

Guy, H. P. (1970). Fluvial sediment concepts. *Techniques of Water-Resources Investigations of the U.S. Geological Survey 03-C1* (55 pp.). https://doi.org/10.3133/twri03C1

Hazel, J. E., Jr., Topping, D. J., Schmidt, J. C., & Kaplinski, M. (2006). Influence of a dam on fine-sediment storage in a canyon river. *Journal of Geophysical Research*, *111*, F01025. https://doi.org/10.1029/2004JF000193

Helsel, D. R., & Hirsch, R. M. (2002). Statistical methods in water resources. *Techniques of Water-Resources Investigations of the United States Geological Survey 04-A3* (510 pp.). https://doi.org/10.3133/twri04A3

Hirsch, R. M. (1988). Statistical methods and sampling design for estimating step trends in surface-water quality. *Water Resources Bulletin*, *24*, 493–503. https://doi.org/10.1111/j.1752-1688.1988.tb00899.x

Horowitz, A. J. (2003). An evaluation of sediment rating curves for estimating suspended sediment concentrations for subsequent flux calculations. *Hydrological Processes*, *17*, 3387–3409. https://doi.org/10.1002/hyp.1299

Horowitz, A. J., Clarke, R. T., & Merten, G. H. (2015). The effects of sample scheduling and sample numbers on estimates of the annual fluxes of suspended sediment in fluvial systems. *Hydrological Processes*, *29*, 531–543. https://doi.org/10.1002/hyp.10172

Howard, A., & Dolan, R. (1981). Geomorphology of the Colorado River in the Grand Canyon. *Journal of Geology*, *89*, 269–298. https://doi.org/10.1086/628592

Howard, A. D. (1994). A detachment-limited model of drainage basin evolution. *Water Resources Research*, *30*, 2261–2285. https://doi.org/10.1029/94WR00757

Kaplinski, M., Hazel, J. E., Jr., Gushue, T., Buscombe, D. D., Kohl, K., & Grams, P. E. (2020a). Channel Mapping of the Colorado River in Grand Canyon National Park, Arizona – April 2011, river miles 61 to 88—Data. *U.S. Geological Survey Data Release*. https://doi.org/10.5066/P95BA2Y1

Kaplinski, M., Hazel, J. E., Jr, Gushue, T., Buscombe, D. D., Kohl, K., & Grams, P. E. (2020b). Channel Mapping of the Colorado River in Grand Canyon National Park, Arizona – May 2014, river miles 61 to 88—Data. *U.S. Geological Survey Data Release*. https://doi.org/10.5066/P99SSSU6

Kiang, J. E., Mason, R. R., & Cohn, T. A. (2016). A survey of the uncertainty in stage-discharge rating curves and streamflow records in the United States. In G. Constantinescu, M. Garcia, & D. Hanes (Eds.), *River Flow 2016, CD-ROM Proceedings of the International Conference on Fluvial Hydraulics, St. Louis, MO, July 11–14* (pp. 724–728). New York, NY: CRC Press, Taylor & Francis Group.

Krumbein, W. C. (1934). Size frequency distributions of sediments. *Journal of Sedimentary Petrology*, *2*, 65–77. https://doi.org/10.1306/D4268EB9-2B26-11D7-8648000102C1865D

Laursen, E. M., Ince, S., & Pollack, J. (1976). On sediment transport through the Grand Canyon. *Proceedings of the 3rd Federal Interagency Sedimentation Conference, March 22–25, Denver, CO* (pp. 4-76–4-87). Retrieved from https://acwi.gov/sos/pubs/3rdFISC/3FiscTOC.PDF

Lisle, T. E. (1989). Sediment transport and resulting deposition in spawning gravels, north coastal California. *Water Resources Research*, *25*, 1303–1319. https://doi.org/10.1029/WR025i006p01303

Lisle, T. E. (2007). The evolution of sediment waves influenced by varying transport capacity in heterogeneous rivers. In H. Habersack, H. Piegay, & M. Rinaldi (Eds.), *Gravel-Bed Rivers VI: From Process Understanding to River Restoration, Developments in Earth Surface Processes, 11* (pp. 443–469). https://doi.org/10.1016/S0928-2025(07)11136-6

Long, C. E., Wiberg, P. L., & Nowell, A. R. M. (1993). Evaluation of von Karman's constant from integral flow parameters. *Journal of Hydraulic Engineering*, *119*, 1182–1190. https://doi.org/10.1061/(ASCE)0733-9429

Love, S. K. (1966). Quality of the Surface Waters of the United States 1963, Parts 9-14. Colorado River Basin to Pacific Slope Basins in Oregon and lower Columbia River Basin. *U.S. Geological Survey Water-Supply Paper 1951* (781 pp.). https://doi.org/10.3133/wsp1951

McLean, S. R. (1992). On the calculation of suspended load for noncohesive sediments. *Journal of Geophysical Research*, *97*, 5759–5770. https://doi.org/10.1029/91JC02933

Melis, T. S., Phillips, W. M., Webb, R. H., & Bills, D. J. (1996). When the blue-green waters turn red: Historical flooding in Havasu Creek, Arizona. *U.S. Geological Survey Water-Resources Investigations Report 96-4059* (136 pp.). https://doi.org/10.3133/wri964059

Milliman, J. D., & Meade, R. H. (1983). World-wide delivery of river sediment to the oceans. *Journal of Geology*, *91*, 1–21. https://doi.org/10.1086/628741

Mohrig, D., & Smith, J. D. (1996). Predicting the migration rates of subaqueous dunes. *Water Resources Research*, *32*, 3207–3217. https://doi.org/10.1029/96WR01129

Montgomery, D. R. (2003). *King of fish: The thousand-year run of salmon*. Cambridge, MA: Westview Press.

Naqshband, S., Hoitink, A. J. F., McElroy, B., Hurther, D., & Hulscher, S. J. M. H. (2017). A sharp view on river dune transition to upper stage plane bed. *Geophysical Research Letters*, *44*, 11437–11444. https://doi.org/10.1002/2017GL075906

Naqshband, S., McElroy, B., & Mahon, R. C. (2017). Validating a universal model of particle transport lengths with laboratory measurements of suspended grain motions. *Water Resources Research*, *53*, 4106–4123. https://doi.org/10.1002/2016WR020024

O'Connor, J. E., Ely, L. L., Wohl, E. E., Stevens, L. E., Melis, T. S., Kale, V. S., & Baker, V. R. (1994). A 4500-year record of large floods on the Colorado River in the Grand Canyon, Arizona. *Journal of Geology*, *102*, 1–9. https://doi.org/10.1086/629644

Osmundson, D. B., Ryel, R. J., Lamarra, V. L., & Pitlick, J. (2002). Flow–sediment–biota relations: Implications for river regulation effects on native fish abundance. *Ecological Applications*, *12*, 1719–1739. https://doi.org/10.1890/1051-0761(2002)012[1719:FSBRIF]2.0.CO;2

Paola, C., & Voller, V. R. (2005). A generalized Exner equation for sediment mass balance. *Journal of Geophysical Research*, *110*, F04014. https://doi.org/10.1029/2004JF000274

Parker, G. (1978). Self-formed straight rivers with equilibrium banks and mobile bed. Part 1: The sand-silt river. *Journal of Fluid Mechanics*, *89*, 109–125. https://doi.org/10.1017/S0022112078002499

Parker, G. (1991). Selective sorting and abrasion of river gravel. I: Theory. *Journal of Hydraulic Engineering*, *117*, 131–149. https://doi.org/10.1061/(ASCE)0733-9429(1991)117:2(131)

Parker, G., Paola, C., & Leclair, S. (2000). Probabilistic Exner sediment continuity equation for mixtures with no active layer. *Journal of Hydraulic Engineering*, *126*, 818–826. https://doi.org/10.1061/(ASCE)0733-9429(2000)126:11(818)

Pizzuto, J., Keeler, J., Skalak, K., & Karwan, D. (2017). Storage filters upland suspended sediment signals delivered from watersheds. *Geology*, *45*, 151–154. https://doi.org/10.1130/G38170.1

Platt, A. S. (2018). *Estimating riverbed sand thickness using CHIRP sonar: Case study from the Colorado River in Grand Canyon* (M.S. thesis). University of Northern Arizona.

Porterfield, G. (1972). Computation of fluvial sediment discharge. *Techniques of Water-Resources Investigations of the U.S. Geological Survey 03-C3* (66 pp.). https://doi.org/10.3133/twri03C3

Rattray, M., Jr., & Mitsuda, E. (1974). Theoretical analysis of conditions in a salt wedge. *Estuarine Coastal Marine Science*, *2*, 373–394. https://doi.org/10.1016/0302-3524(74)90006-1

Rote, J. J., Flynn, M. E., & Bills, D. J. (1997). Hydrologic data, Colorado River and major tributaries, Glen Canyon Dam to Diamond Creek, Arizona, water years 1990–95. *U.S. Geological Survey Open-File Report 97–250* (474 pp.). https://doi.org/10.3133/ofr97250

Rouse, H. (1937). Modern conceptions of mechanics of fluid turbulence. *Transactions of the American Society of Civil Engineers*, *102*, 463–505.

Rubin, D. M., Anima, R. A., & Sanders, R. (1994). Measurements of sand thicknesses in Grand Canyon, Arizona, and a conceptual model for characterizing changes in sand-bar volume through time and space. *U.S. Geological Survey Open-File Report 94-597* (9 pp.). https://doi.org/10.3133/ofr94597

Rubin, D. M., Buscombe, D., Wright, S. A., Topping, D. J., Grams, P. E., Schmidt, J. C., et al. (2020). Causes of variability in suspended-sand concentration evaluated using measurements in the Colorado River in Grand Canyon. *Journal of Geophysical Research: Earth Surface*, *125*, e2019JF005226. https://doi.org/10.1029/2019JF005226

Rubin, D. M., & Hunter, R. E. (1982). Bedform climbing in theory and nature. *Sedimentology*, *29*, 121–138. https://doi.org/10.1111/j.1365-3091.1982.tb01714.x

Rubin, D. M., Nelson, J. M., & Topping, D. J (1998). Relation of inversely graded deposits to suspended-sediment grain-size evolution during the 1996 Flood Experiment in Grand Canyon. *Geology*, *26*, 99–102. https://doi.org/10.1130/0091-7613(1998)026<0099:ROIGDT>2.3.CO;2

Rubin, D. M., Schmidt, J. C., & Moore, J. N. (1990). Origin, structure, and evolution of a reattachment bar, Colorado River, Grand Canyon, Arizona. *Journal of Sedimentary Petrology*, *60*, 982–991. http://dx.doi.org/10.1306/D426765E-2B26-11D7-8648000102C1865D

Rubin, D. M., Tate, G. M., Topping, D. J., & Anima, R. A. (2001). Use of rotating side-scan sonar to measure bedload. *Proceedings of the 7th Interagency Sedimentation Conference, March 25–29* (Vol. 1, pp. III-139–III-143). Reno, NV. Retrieved from http://pubs.usgs.gov/misc_reports/FISC_1947-2006/pdf/1st-7thFISCs-CD/7thFISC/7Fisc-V1/7FISC1-3.pdf

Rubin, D. M., & Topping, D. J. (2001). Quantifying the relative importance of flow regulation and grain-size regulation of suspended-sediment transport α, and tracking changes in bed-sediment grain size β. *Water Resources Research*, *37*, 133–146. https://doi.org/10.1029/2000WR900250

Rubin, D. M., & Topping, D. J. (2008). Correction to "Quantifying the relative importance of flow regulation and grain-size regulation of suspended-sediment transport α, and tracking changes in bed-sediment grain size β". *Water Resources Research*, *44*, W09701. https://doi.org/10.1029/2008WR006819

Rubin, D. M., Topping, D. J., Schmidt, J. C., Hazel, J., Kaplinski, K., & Melis, T. S. (2002). Recent sediment studies refute Glen Canyon Dam hypothesis. *EOS, Transactions of the American Geophysical Union*, *83*, 273–278. https://doi.org/10.1029/2002EO000191

Sabol, T. A., & Topping, D. J. (2013). Evaluation of intake efficiencies and associated sediment-concentration errors in US D-77 bag-type and US D-96-type depth-integrating suspended-sediment samplers. *U.S. Geological Survey Scientific Investigations Report 2012-5208* (88 pp.). https://doi.org/10.3133/sir20125208

Sauer, V. B., & Meyer, R. W. (1992). Determination of error in individual discharge measurements. *U.S. Geological Survey Open-File Report 92-144* (21 pp.). Retrieved from http://pubs.usgs.gov/of/1992/ofr92-144/

Schmidt, J. C. (1990). Recirculating flow and sedimentation in the Colorado River in Grand Canyon, Arizona. *Journal of Geology*, *98*, 709–724. https://doi.org/10.1086/629435

Schmidt, J. C., & Graf, J. B. (1990). Aggradation and degradation of alluvial sand deposits, 1965 to 1986, Colorado River, Grand Canyon National Park, Arizona. *U.S. Geological Survey Professional Paper 1493* (74 pp.). https://doi.org/10.3133/pp1493

Schmidt, J. C., & Grams, P. E. (2011). Understanding physical processes of the Colorado River. In T. S. Melis (Ed.), *Effects of three high-flow experiments on the Colorado River ecosystem downstream from Glen Canyon Dam, Arizona. U.S. Geological Survey Circular 1366* (pp. 17–52). Retrieved from https://pubs.usgs.gov/circ/1366/

Schmidt, J. C., Grams, P. E., & Leschin, M. F. (1999). Variation in the magnitude and style of deposition and erosion in three long (8–12 km) reaches as determined by photographic analysis. In R. H. Webb, J. C. Schmidt, G. R. Marzolf, & R. A. Valdez (Eds.), *The Controlled Flood in Grand Canyon, Geophysical Monograph*, 110 (pp. 185–203). Washington, DC: American Geophysical Union. https://doi.org/10.1029/GM110p0185

Schmidt, J. C., & Rubin, D. M. (1995). Regulated streamflow, fine-grained deposits, and effective discharge in canyons with abundant debris fans. In J. E. Costa, A. J. Miller, K. W. Potter, & P. R. Wilcock (Eds.), *Natural and anthropogenic influences in fluvial geomorphology: The Wolman Volume, Geophysical Monograph*, 89 (pp. 177–195). Washington, DC: American Geophysical Union. https://doi.org/10.1029/GM089p0177

Schmidt, J. C., Rubin, D. M., & Ikeda, H. (1993). Flume simulations of recirculating flow and sedimentation. *Water Resources Research*, *29*, 2925–2939. https://doi.org/10.1029/93WR00770

Schmidt, J. C., Topping, D. J., Grams, P. E., & Hazel, J. E. (2004). System-wide changes in the distribution of fine sediment in the Colorado River corridor between Glen Canyon Dam and Bright Angel Creek, Arizona. *Final report to the U.S. Geological Survey Grand Canyon Monitoring and Research Center* (107 pp.). Flagstaff, AZ. Retrieved from https://www.usbr.gov/uc/progact/amp/amwg/2005-03-02-amwg-meeting/Attach_05a.pdf

Schmidt, J. C., Topping, D. J., Rubin, D. M., Hazel, J. E., Jr., Kaplinski, M., Wiele, S. M., & Goeking, S. A. (2007). Streamflow and sediment data collected to determine the effects of Low Summer Steady Flows and Habitat Maintenance Flows in 2000 on the Colorado River between Lees Ferry and Bright Angel Creek, Arizona. *U.S. Geological Survey Open-File Report 2007-1268* (79 pp.). https://doi.org/10.3133/ofr20071268

Schmidt, J. C., & Wilcock, P. R. (2008). Metrics for assessing the downstream effects of dams. *Water Resources Research*, *44*, W04404. https://doi.org/10.1029/2006WR005092

Sibley, D., Topping, D. J., Hines, M., & Garner, B. (2015). User-interactive sediment budgets in a browser: A web application for river science and management. *Proceedings of the 3rd Joint Federal Interagency Conference on Sedimentation and Hydrologic Modeling, April 19–23* (pp. 595–605). Reno, NV: Peppermill Hotel. Retrieved from https://acwi.gov/sos/pubs/3rdJFIC/Contents/4A-Sibley.pdf

Skalak, K., & Pizzuto, J. (2010). The distribution and residence time of suspended sediment stored within the channel margins of a gravel-bed bedrock river. *Earth Surface Processes and Landforms*, *35*, 435–446. https://doi.org/10.1002/esp.1926

Sklar, L. S., & Dietrich, W. E. (2001). Sediment and rock strength controls on river incision into bedrock. *Geology*, *29*, 1987–1090. https://doi.org/10.1130/0091-7613(2001)029<1087:SARSCO>2.0.CO;2

Smith, J. D. (1970). Stability of a sand bed subjected to a shear flow of low Froude number. *Journal of Geophysical Research*, *75*, 5928–5940. https://doi.org/10.1029/JC075i030p05928

Taylor, J. R. (1997). *An introduction to error analysis: The study of uncertainties in physical measurements*. 2nd ed. Sausalito, CA: University Science Books.

Topping, D. J. (1997). *Physics of flow, sediment transport, hydraulic geometry, and channel geomorphic adjustment during flash floods in an ephemeral river, the Paria River, Utah and Arizona* (Ph.D. thesis). University of Washington.

Topping, D. J., Grams, P. E., Griffiths, R. E., Hazel, J. E., Jr., Kaplinski, M., Dean, D. J., et al. (2019). Optimal timing of high-flow experiments for sandbar deposition. U.S. Bureau of Reclamation, Glen Canyon Dam Adaptive Management Program. *High-Flow Experiments Assessment Extended Abstracts, March 2019 Annual Reporting Meeting*, March 6–7, Tempe, AZ (pp. 3–9). Retrieved from https://pubs.er.usgs.gov/publication/70203738 or https://www.usbr.gov/uc/progact/amp/amwg/2019-03-06-amwg-meeting/20190301-HFE_Extended_Abstracts-Combined_FINAL.pdf

Topping, D. J., Mueller, E. R., Schmidt, J. C., Griffiths, R. E., Dean, D. J., & Grams, P. E. (2018). Long-term evolution of sand transport through a river network: Relative influences of a dam versus natural changes in grain size from sand waves. *Journal of Geophysical Research: Earth Surface*, *123*, 1879–1909. https://doi.org/10.1029/2017JF004534

Topping, D. J., Rubin, D. M., Grams, P. E., Griffiths, R. E., Sabol, T. A., Voichick, N., et al. (2010). Sediment transport during three controlled-flood experiments on the Colorado River downstream from Glen Canyon Dam, with implications for eddy-sandbar deposition in Grand Canyon National Park. *U.S. Geological Survey Open-File Report 2010-1128* (111 pp.). https://doi.org/10.3133/ofr20101128

Topping, D. J., Rubin, D. M., & Melis, T. S. (2007). Coupled changes in sand grain size and sand transport driven by changes in the upstream supply of sand in the Colorado River: Relative importance of changes in bed-sand grain size and bed-sand area. *Sedimentary Geology*, *202*, 538–561. https://doi.org/10.1016/j.sedgeo.2007.03.016

Topping, D. J., Rubin, D. M., Nelson, J. M., Kinzel, P. J., III, & Bennett, J. P. (1999). Linkage between grain-size evolution and sediment depletion during Colorado River floods. In R. H. Webb, J. C. Schmidt, G. R. Marzolf, & R. A. Valdez (Eds.), *The 1996 Controlled Flood in Grand Canyon, Geophysical Monograph*, 110 (pp. 71–98). Washington, DC: American Geophysical Union. https://doi.org/10.1029/GM110p0071

Topping, D. J., Rubin, D. M., Nelson, J. M., Kinzel, P. J., III, & Corson, I. C. (2000). Colorado River sediment transport 2. Systematic bed-elevation and grain-size effects of sand supply limitation. *Water Resources Research*, *36*, 543–570. https://doi.org/10.1029/1999WR900286

Topping, D. J., Rubin, D. M., & Schmidt, J. C. (2005). Regulation of sand transport in the Colorado River by changes in the surface grain size of eddy sandbars over multi-year timescales. *Sedimentology*, *52*, 1133–1153. https://doi.org/10.1111/j.1365-3091.2005.00738.x

Topping, D. J., Rubin, D. M., & Schmidt, J. C. (2008). Update on regulation of sand transport in the Colorado River by changes in the surface grain size of eddy sandbars over multiyear timescales. *U.S. Geological Survey Scientific Investigations Report 2008-5042* (24 pp.). https://doi.org/10.3133/sir20085042

Topping, D. J., Rubin, D. M., Schmidt, J. C., Hazel, J. E., Jr., Melis, T. S., Wright, S. A., et al. (2006). Comparison of sediment-transport and bar-response results from the 1996 and 2004 controlled-flood experiments on the Colorado River in Grand Canyon. *Proceedings of the 8th Federal Interagency Sedimentation Conference, April 2–6. Reno, NV*. Retrieved from http://acwi.gov/sos/pubs/8thFISC/Session1B-3_Topping.pdf

Topping, D. J., Rubin, D. M., & Vierra, L. E., Jr. (2000). Colorado River sediment transport 1. Natural sediment supply limitation and the influence of Glen Canyon Dam. *Water Resources Research*, *36*, 515–542. https://doi.org/10.1029/1999WR900285

Topping, D. J., Rubin, D. M., Wright, S. A., & Melis, T. S. (2011). Field evaluation of the error arising from inadequate time averaging in the standard use of depth-integrating suspended-sediment samplers. *U.S. Geological Survey Professional Paper 1774* (95 pp.). https://doi.org/10.3133/pp1774

Topping, D. J., Schmidt, J. C., & Vierra, L. E. Jr. (2003). Computation and analysis of the instantaneous-discharge record for the Colorado River at Lees Ferry, Arizona—May 8, 1921, through September 30, 2000. *U.S. Geological Survey Professional Paper 1677* (118 pp.). https://doi.org/10.3133/pp1677

Topping, D. J., & Wright, S. A. (2016). Long-term continuous acoustical suspended-sediment measurements in rivers – Theory, application, bias, and error. *U.S. Geological Survey Professional Paper 1823* (98 pp.). https://doi.org/10.3133/pp1823.98

Topping, D. J., Wright, S. A., Griffiths, R. E., & Dean, D. J. (2016). Long-term continuous acoustical suspended-sediment measurements in rivers – Theory, evaluation, and results from 14 stations on five rivers. In G. Constantinescu, M. Garcia, & D. Hanes (Eds.), *River Flow 2016, CD-ROM Proceedings of the International Conference on Fluvial Hydraulic*, St. Louis, MO, July 11–14 (pp. 1510–1518). New York, NY: CRC Press, Taylor & Francis Group.

U.S. Department of the Interior. (1995). *Operation of Glen Canyon Dam – Final Environmental Impact Statement, Colorado River Storage Project*, Arizona. Salt Lake City, UT: Bureau of Reclamation, Upper Colorado Region (337 pp.). Retrieved from https://www.usbr.gov/uc/envdocs/eis/gc/gcdOpsFEIS.html

U.S. Department of the Interior. (1996). *Record of Decision, Operation of Glen Canyon Dam – Final Environmental Impact Statement*. Washington, DC: Office of the Secretary of the Interior (15 pp.). Retrieved from https://www.usbr.gov/uc/envdocs/rod/Oct1996_OperationGCD_ROD.pdf

U.S. Department of the Interior. (2016a). *Glen Canyon Dam Long-term Experimental and Management Plan Environmental Impact Statement*. Salt Lake City, UT: Bureau of Reclamation, Upper Colorado Region; Lakewood, CO: National Park Service, Intermountain Region. Retrieved from http://ltempeis.anl.gov

U.S. Department of the Interior. (2016b). *Record of Decision for the Glen Canyon Dam Long-term Experimental and Management Plan Environmental Impact Statement*. Washington, DC: Office of the Secretary of the Interior; Salt Lake City, UT: Bureau of Reclamation, Upper Colorado Region, Lakewood, CO: National Park Service, Intermountain Region (15 pp. plus appendices). Retrieved from http://ltempeis.anl.gov/documents/docs/LTEMP_ROD.pdf

U.S. Geological Survey. (1969). Quality of the Surface Waters of the United States 1964, Parts 9-11. Colorado River Basin to Pacific Slope Basins in California. *U.S. Geological Survey Water-Supply Paper 1958* (615 pp.). https://doi.org/10.3133/wsp1958

U.S. Geological Survey. (1970). Quality of the Surface Waters of the United States 1965, Parts 9-11. Colorado River Basin to Pacific Slope Basins in California. *U.S. Geological Survey Water-Supply Paper 1965* (678 pp.). https://doi.org/10.3133/wsp1965

U.S. Geological Survey. (2019a). *Streamflow Measurements for the Nation*. Retrieved from https://waterdata.usgs.gov/nwis/measurements

U.S. Geological Survey. (2019b). *Site Map for the Nation, USGS 09404115 Havasu Creek above the mouth near Supai, AZ*. Retrieved from https://waterdata.usgs.gov/nwis/nwismap/?site_no=09404115&agency_cd=USGS

U.S. Geological Survey. (2019c). *Site Map for the Nation, USGS 09403850 Kanab Creek above the mouth near Supai, AZ*. Retrieved from https://waterdata.usgs.gov/nwis/nwismap/?site_no=09403850&agency_cd=USGS

U.S. Geological Survey. (2019d). *Site Map for the Nation, USGS 09403780 Kanab Creek near Fredonia, AZ*. Retrieved from https://waterdata.usgs.gov/nwis/nwismap/?site_no=09403780&agency_cd=USGS

U.S. Geological Survey. (2020). *USGS Water-Quality Data for the Nation*. Retrieved from https://waterdata.usgs.gov/nwis/qw

Venditti, J. G., Rennie, C. D., Bonhof, J., Bradley, R. W., Little, M., & Church, M. (2014). Flow in bedrock canyons. *Nature*, *513*, 534–537. https://doi.org/10.1038/nature13779

von Karman, T. (1930). Mechanische Ähnlichkeit und Turbulenz. *Nachrichten von der Gesellschaft der Wissenschaften zu Göttingen, Mathematisch-Physikalische Klasse*, 58–76. Retrieved from http://resolver.sub.uni-goettingen.de/purl?PPN252457811_1930 [Reprinted as Mechanical Similitude and Turbulence, *National Advisory Committee for Aeronautics (NACA) Technical Memorandum 611*, 21 pp., 1931. https://ntrs.nasa.gov/citations/19930094805

Webb, R. H., Griffiths, P. G., Melis, T. S., & Hartley, D. R. (2000). Sediment delivery by ungaged tributaries of the Colorado River in Grand Canyon, Arizona. *U.S. Geological Survey Water-Resources Investigations Report 2000-4055* (pp. 67). https://doi.org/10.3133/wri004055

Webb, R. H., Schmidt, J. C., Marzolf, G. R., & Valdez, R. A. (Eds.). (1999). *The 1996 Controlled Flood in Grand Canyon, Geophysical Monograph*, 110. Washington, DC: American Geophysical Union (367 pp.). https://doi.org/10.1029/GM110

Woo, H. S., Julien, P. Y., & Richardson, E. V. (1986). Washload and fine sediment load. *Journal of Hydraulic Engineering*, *112*, 541–545. https://doi.org/10.1061/(ASCE)0733-9429(1986)112:6(541)

Whipple, K. X., DiBiase, R. A., & Crosby, B. T. (2013). Bedrock rivers. In J. Shroder & E. Wohl (Eds.), *Treatise on Geomorphology, 9, Fluvial Geomorphology* (pp. 550–573). San Diego, CA: Academic Press. https://doi.org/10.1016/B978-0-12-374739-6.00254-2

Whipple, K. X., Hancock, G. S., & Anderson, R. S. (2000). River incision into bedrock: Mechanics and relative efficacy of plucking, abrasion, and cavitation. *Geological Society of America Bulletin*, *112*, 490–503. https://doi.org/10.1130/0016-7606(2000)112<490:RIIBMA>2.0.CO;2

Wiberg, P. L., & Smith, J. D. (1991). Velocity distribution and bed roughness in high-gradient streams. *Water Resources Research*, *27*, 825–838. https://doi.org/10.1029/90WR02770

Wright, S. A., & Kennedy, T. A. (2011). Science-based strategies for future high-flow experiments at Glen Canyon Dam. In T. S. Melis (Ed.), *Effects of three high-flow experiments on the Colorado River ecosystem downstream from Glen Canyon Dam, Arizona, U.S. Geological Survey Circular 1366* (pp. 127–147). Retrieved from https://pubs.usgs.gov/circ/1366/

Wright, S. A., Schmidt, J. C., Melis, T. S., Topping, D. J., & Rubin, D. M. (2008). Is there enough sand? Evaluating the fate of Grand Canyon sandbars. *GSA Today*, *18*, 4–10. https://doi.org/10.1130/GSATG12A.1

Wright, S. A., Topping, D. J., Rubin, D. M., & Melis, T. S. (2010). An approach for modeling sediment budgets in supply-limited rivers. *Water Resources Research*, *46*, W10538. https://doi.org/10.1029/2009WR008600

Erratum

The originally published version of this article included several typographical errors in which a variable was used when words were needed. These errors have been corrected, and this may be considered the official version of record.